AD-A048 582 SRI INTERNATIONAL MENLO PARK CALIF F/G 11/2
MICROWAVE TECHNIQUES FOR NONDESTRUCTIVE EVALUATION OF CERAMICS.(U)
NOV 77 A J BAHR DAAG46-76-C-0048
UNCLASSIFIED AMMRC-CTR-77-29 NL

1 OF 1
ADA048582

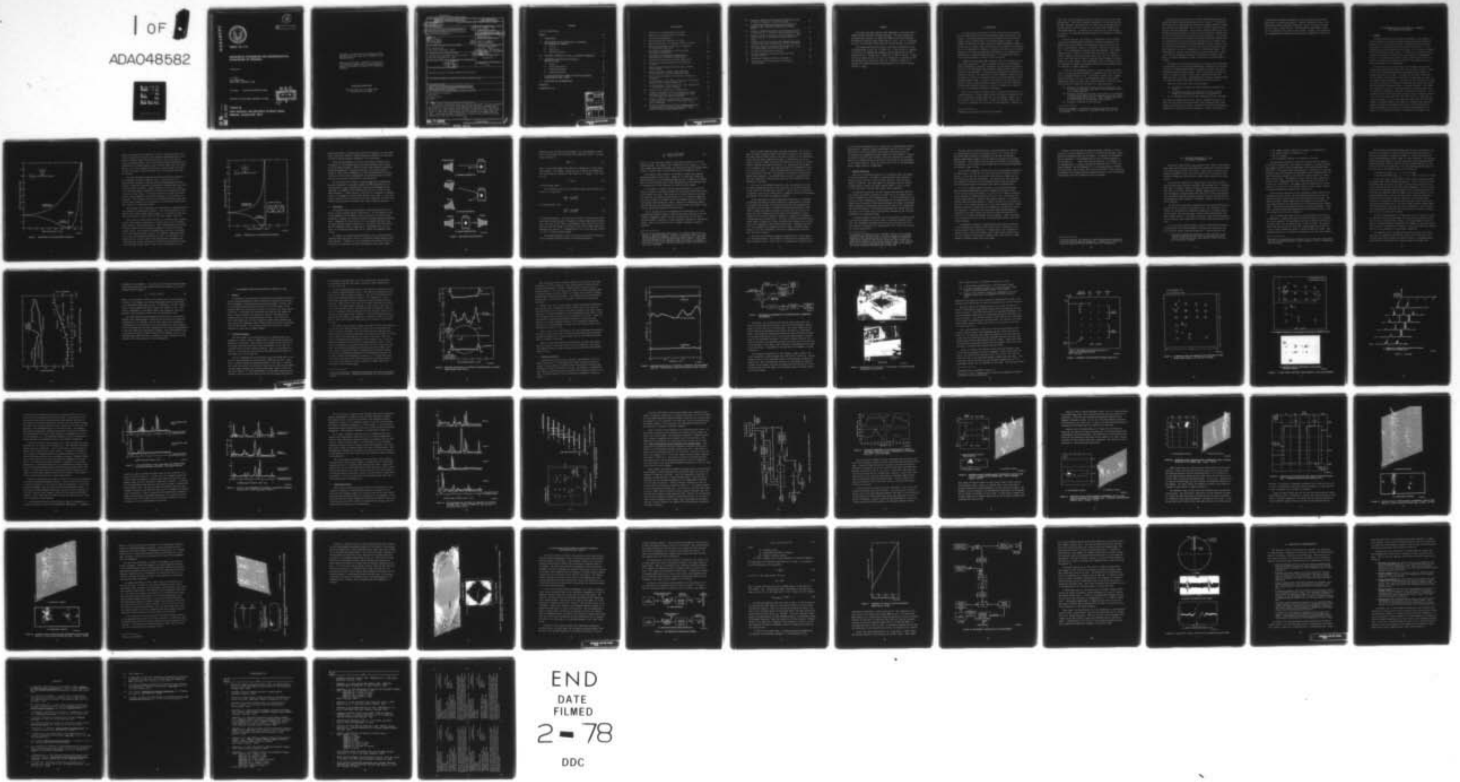

END
DATE
FILMED
2-78
DDC

ADA048582

(12) B.S.

AD

AMMRC CTR 77-29

MICROWAVE TECHNIQUES FOR NONDESTRUCTIVE EVALUATION OF CERAMICS

November 1977

A. J. BAHR
SRI INTERNATIONAL
MENLO PARK, CALIFORNIA 94025

Final Report *Contract Number DAAG46-76-C-0048*

DDC
RECEIVED
JAN 9 1978
B

Approved for public release; distribution unlimited.

AD No. ____
DDC FILE COPY

Prepared for

ARMY MATERIALS AND MECHANICS RESEARCH CENTER
Watertown, Massachusetts 02172

The findings in this report are not to be construed as an official Department of the Army position, unless so designated by other authorized documents.

Mention of any trade names or manufacturers in this report shall not be construed as advertising nor as an official indorsement or approval of such products or companies by the United States Government.

DISPOSITION INSTRUCTIONS

Destroy this report when it is no longer needed.
Do not return it to the originator.

UNCLASSIFIED

SECURITY CLASSIFICATION OF THIS PAGE (When Data Entered)

REPORT DOCUMENTATION PAGE		READ INSTRUCTIONS BEFORE COMPLETING FORM
1. REPORT NUMBER AMMRC CTR-77-29	2. GOVT ACCESSION NO.	3. RECIPIENT'S CATALOG NUMBER
4. TITLE (and Subtitle) MICROWAVE TECHNIQUES FOR NONDESTRUCTIVE EVALUATION OF CERAMICS		5. TYPE OF REPORT & PERIOD COVERED Final Report, Covering the Period 30 June 1976 to 30 August 77
		6. PERFORMING ORG. REPORT NUMBER Final Report SRI Project 5594
7. AUTHOR(s) Alfred J. Bahr		8. CONTRACT OR GRANT NUMBER(s) DAAG46-76-C-0048
9. PERFORMING ORGANIZATION NAME AND ADDRESS SRI International Menlo Park, California 94025		10. PROGRAM ELEMENT, PROJECT, TASK AREA & WORK UNIT NUMBERS D/A Proj: M766350 AMCMS Code: 5397-0M-6350
11. CONTROLLING OFFICE NAME AND ADDRESS Army Materials and Mechanics Research Center Watertown, Massachusetts 02172		12. REPORT DATE November 1977 13. NO. OF PAGES 76
14. MONITORING AGENCY NAME & ADDRESS (if diff. from Controlling Office) (12) 71p.		15. SECURITY CLASS. (of this report) Unclassified 15a. DECLASSIFICATION/DOWNGRADING SCHEDULE N/A

16. DISTRIBUTION STATEMENT (of this report)

Approved for public release; distribution unlimited.

17. DISTRIBUTION STATEMENT (of the abstract entered in Block 20, if different from report)

18. SUPPLEMENTARY NOTES

This project has been accomplished as part of the U. S. Army Materials Testing Technology Program, which has for its objective the timely establishment of testing techniques procedures or prototype equipment (in mechanical, chemical, or nondestructive testing) to insure efficient inspection methods for materiel/material procured or maintained by DARCOM.

19. KEY WORDS (Continue on reverse side if necessary and identify by block number)

Nondestructive evaluation
Microwaves
Silicon nitride
Ceramics

20. ABSTRACT (Continue on reverse side if necessary and identify by block number)

The ability of microwave energy to penetrate some kinds of ceramic materials at frequencies of 100 GHz and above suggests that microwave techniques may be useful for the nondestructive evaluation (NDE) of such materials. The work described in this report demonstrates the basic feasibility of using these techniques to detect and locate various types of inclusions (including voids) in Si_3N_4. Inclusions as small as 0.005 inch in diameter have been detected using frequencies in the range 50 to 100 GHz.

DD FORM 1 JAN 73 1473

EDITION OF 1 NOV 65 IS OBSOLETE

UNCLASSIFIED

SECURITY CLASSIFICATION OF THIS PAGE (When Data Entered)

410 281

CONTENTS

LIST OF ILLUSTRATIONS v

PREFACE vii

I INTRODUCTION 1

II CONSIDERATIONS IN THE SELECTION OF A MICROWAVE NDE TECHNIQUE FOR CERAMICS 5

A. General 5

B. Sensitivity 9

C. Spatial Resolution 14

III DIELECTRIC PROPERTIES OF Si_3N_4 AT MICROWAVE FREQUENCIES. . . 17

IV EXPERIMENTAL DETECTION AND LOCATION OF DEFECTS IN Si_3N_4 23

A. General 23

B. K-Band Measurements 23

C. V-Band Measurements 26

D. W-Band Measurements 38

V AN OSCILLATOR-PULLING SCHEME FOR DETECTING MICROWAVE BACKSCATTERING FROM A DEFECT 55

VI CONCLUSIONS AND RECOMMENDATIONS 63

REFERENCES 65

DISTRIBUTION LIST 67

ACCESSION for
NTIS White Section ☑
DDC Buff Section ☐
UNANNOUNCED ☐
JUSTIFICATION
BY
DISTRIBUTION/AVAILABILITY CODES
Dist. AVAIL. and/or SPECIAL
A

PRECEDING PAGE NOT FILMED BLANK

ILLUSTRATIONS

1 Reflection at an Air/Dielectric Interface 6

2 Reflection at a Dielectric/Air Interface 8

3 Scattering Configurations 10

4 Measured Dielectric Properties of Si_3N_4 20

5 Measured Scattering as a Function of Probe Position 25

6 Measured Scattering as a Function of Frequency for Hot-Pressed Si_3N_4 Disk 27

7 Experimental Arrangement for Cross-Polarized Transmission Measurements 28

8 Photographs of Experimental Arrangement for Cross-Polarized Transmission Measurements 29

9 Intended Flaw Locations for Seeded Si_3N_4 Billet 31

10 Ultrasonic C-Scan Map Showing Actual Positions of Flaws 32

11 Typical Results Obtained Using Microwave (V-Band) C-Scan Mapping 33

12 Typical Microwave (V-Band) C-Scan Amplitude Presentations for Large and Small Inclusions 36

13 Typical V-Band Responses for Different Illumination Techniques 37

14 An Illustration of the Effect of Frequency on Detected Response Using a Pinhole Transmitter 39

15 An Illustration of the Detection of a Flaw Not Detected by the Ultrasonic C-Scan Technique 40

16 System for the Acquisition of Sampled Data 42

17 Frequency Dependence of the Cross-Polarized Forward Scattering from Four Types of Inclusions in a Hot-Pressed Si_3N_4 Plate--Billet E307103897 43

18 Microwave (W-Band) Cross-Polarized Transmission C-Scan of Four Types of Inclusions in Hot-Pressed Si_3N_4--Billet E307103897 44

19 Microwave (W-Band) Cross Polarized Transmission C-Scan of Four Types of Inclusions in Hot-Pressed Si_3N_4--AiResearch Manufacturing Company Billet 45

PRECEDING PAGE NOT FILMED BLANK

20 Microwave (W-Band) Cross-Polarized Transmission C-Scan of Silicon Inclusions in Hot-Pressed Si_3N_4 46

21 Intended Flaw Locations and Scan Areas in Reaction-Sintered Si_3N_4--AiResearch Manufacturing Company Billet 47

22 Microwave (W-Band) Cross-Polarized Transmission C-Scan of Scan Area No. 1 (Si-SiC) in Reaction-Sintered Si_3N_4 . . . 48

23 Microwave (W-Band) Cross-Polarized Transmission C-Scan of Scan Area No. 2 (C-voids) in Reaction-Sintered Si_3N_4 49

24 Microwave (W-Band) Cross-Polarized Transmission C-Scan Showing Voids in Hot-Pressed Si_3N_4--Billet F307104930 . . . 51

25 Microwave (W-Band) Cross-Polarized Transmission C-Scan of 4-inch-diameter Hot-Pressed Si_3N_4 Disk 53

26 Two Monostatic-Backscatter Schemes 56

27 Frequency Deviation vs Relative Reflected Power for f_0 = 100 GHz 58

28 Experimental Frequency-Pulling Arrangement 59

29 Detection of a Metal Strip with the Frequency-Pulling Scheme 61

PREFACE

This report has been prepared under Department of the Army Project Number M766350, Materials Testing Technology. The work reported was performed under Contract No. DAAG46-76-C-0048 for the Army Materials and Mechanics Research Center, Watertown, MA 02172. Mr. C. H. Hastings served as the Principal Technologist and contract monitor for the Army.

This program has benefited greatly from ideas contributed by the following people at SRI: Dr. U. Gysel, Dr. T. Itoh, and Mr. L. Robinson. In addition, the experimental apparatus was constructed and the data obtained by Mr. J. Watjen, Mr. P. Evans, Mr. G. Tomlin, and Mr. J. Petro. Particular thanks are also due to Mr. L. Feinstein, a consultant to SRI, who stimulated our interest in this area. Finally, we thank Mr. J. Schuldies of AiResearch Manufacturing Company for the loan of several samples of Si_3N_4.

I INTRODUCTION

In recent years a great deal of effort has gone into the development of ceramic materials for high-performance applications such as gas turbines. The primary materials in this category are silicon nitride (Si_3N_4), silicon carbide (SiC), and lithium-aluminum silicate. Such ceramics are brittle, and their strength is highly dependent on whether defects such as cracks, voids, and inclusions are present in the material. Since it is impossible to completely eliminate such defects, the economic feasibility of using these materials will depend on the availability of nondestructive evaluation (NDE) techniques for locating these defects and determining whether the defects can be tolerated.

A number of conventional NDE techniques have been evaluated for use with ceramic materials.[1*] These techniques include X-ray radiography, neutron radiography, ultrasonic inspection, and dye-penetrant inspection. Of these, X-ray radiography and ultrasonic inspection have probably received the most attention. X-rays have an intrinsically high resolution capability; however, the sensitivity of this technique is limited by the thickness of the piece to be inspected and by the characteristics of the recording medium (film). X-rays are most effective in detecting high-density inclusions such as metallic particles, but they have difficulty in detecting low-density defects or voids. The opposite is claimed to be true for conventional ultrasonic techniques.

There are a number of different types of defects that can occur in ceramic materials. Besides voids, cracks, and density laminations, there can be inclusions of various materials such as tungsten carbide, iron and tungsten, silicon, and carbon. A flaw size of 100 to 200 μm (4 to 12 mils) is considered to be critical at room temperature. However, at

---

* References are listed at the end of this report.

1400°C this critical dimension reduces to about 25 μm (1 mil) for some applications.[2] This latter dimension represents a severe challenge for any NDE technique, especially since the grain size in high-density hot-pressed material can be as large as 5 μm, and as large as 100 μm in cold-formed material. In addition, the criticality of a flaw depends on its type, so a good NDE technique should also be capable of classifying flaws.

It would seem that, in principle, a combination of X-ray radiography and very-high-frequency (100 MHz or greater) ultrasonics[3] can probably meet this demand for high resolution, high sensitivity, and defect classification. However, in practice, there are several problems. X-ray radiography is expensive and time-consuming. The highest frequency that is practical for ultrasonic techniques is limited by surface roughness and grain-boundary scattering. Even for smooth surfaces, great care must be taken in coupling a high-frequency ultrasonic transducer to the ceramic. This requirement makes it difficult to move the transducer or sample for scanning purposes and limits application of the technique to simple geometries.

In view of these limitations there is a need to explore the possibility of using other NDE techniques to complement the X-ray and ultrasonic techniques already in use. One possible candidate for a complementary technique is the use of electromagnetic waves at microwave* frequencies, which, for short, are called microwaves. There are three main reasons for considering microwaves for this application:

(1) Microwaves can penetrate low-loss dielectric materials, and will interact with local variations in the dielectric properties of these materials.

(2) Microwave transducers (antennas) do not need to be in physical contact with the material to be inspected, nor do they require a coupling medium other than air. Thus, scanning rates will be limited primarily by mechanical considerations.

(3) Microwave technology is well advanced.

---

*The term "microwave" is used here to signify frequencies that are greater than 10^9 Hz (1 gigahertz, abbreviated GHz), and less than 3×10^{11} Hz.

The application of microwaves to various NDE problems has been discussed and studied extensively during the last 15 years.[4-6] Microwaves have been used to probe dielectric materials to measure changes in thickness and material composition, and to detect and locate interior flaws such as voids and inclusions. In the case of ceramic turbine parts, the finding and characterization of flaws is of most interest, although there is also a need for quality control in material processing. In the past, the use of microwaves for the detection of small flaws has suffered from the limited sensitivity and resolution capabilities of microwaves that are dictated by the relatively long wavelengths involved. However, this situation has been improved in recent years by the development of microwave components for use at frequencies up to 100 GHz and beyond. The wavelength in a typical ceramic material at these frequencies is about 1 mm, which is beginning to approach the dimension of typical flaws. Hence, it appears worthwhile to take a fresh look at microwave NDE for ceramics.

The objective of the work described in this report was to determine the feasibility of using microwave measurement techniques for detecting, locating, and characterizing defects in ceramic materials, especially hot-pressed silicon nitride (Si_3N_4). Defects of interest included particles of tungsten carbide, iron or steel, unreacted silicon, and graphite, as well as voids. The minimum defect diameter examined during this study was between 0.001 and 0.005 inch (0.025 and 0.127 mm).

There were three basic tasks in this program:

(1) To identify, evaluate, and rank prospective microwave techniques,

(2) To determine the types and magnitudes of defect-related changes in the dielectric properties of Si_3N_4 material,

(3) To implement and test the most promising microwave technique.

The results of addressing the first task are presented in Section II, while the experimental results relevant to the second and third tasks appear in Sections III, IV, and V. Section III discusses the dielectric properties of Si_3N_4 at microwave frequencies. Section IV describes a

cross-polarized microwave transmission system and gives the results of measurements on seeded Si_3N_4 plates. Section V describes a novel cross-polarized microwave reflection system that uses the principle of oscillator pulling to detect defects. Some preliminary experimental results for this system are also given in this section. Finally, the conclusions and recommendations resulting from this work are summarized in Section VI.

II CONSIDERATIONS IN THE SELECTION OF A MICROWAVE NDE TECHNIQUE FOR CERAMICS

A. General

Microwave nondestructive evaluation techniques can be applied to dielectric materials to measure either gross material and geometrical properties (e.g., dielectric constant, dissipation factor, and plate thickness) or localized properties associated with defects.[6] In the evaluation of ceramic materials such as Si_3N_4, one is primarily concerned with the detection of small defects. In this case, the basic principle on which the detection is based is the scattering of electromagnetic waves. The two basic characteristics of the scattered wave that can be measured are amplitude and phase (or delay). These quantities can be measured separately or in combination.

For detection of an interior flaw to be possible, the microwave energy must be able to both enter and leave the ceramic material. First of all, this requirement means that the propagation loss inside the material must not be too large. Secondly, the microwave energy must not be totally reflected from the surface of the material, nor must it be trapped inside the material. The theory for the reflection of a plane wave at an air/dielectric interface[7] shows that some energy will always enter the dielectric material except at grazing incidence. This result is illustrated in Figure 1, where the fraction of incident power that is reflected is plotted as a function of the angle of incidence. It is assumed that the relative dielectric constant of the dielectric material is 7--it will be shown later that this value falls in a range that is typical for Si_3N_4. It can be seen from the figure that, for other than normal or grazing incidence, the fraction of incident power reflected depends on whether the incident wave has its electric-field vector polarized parallel to the plane of incidence or perpendicular to it. Hence, if the electric-field vector is polarized at an angle to the

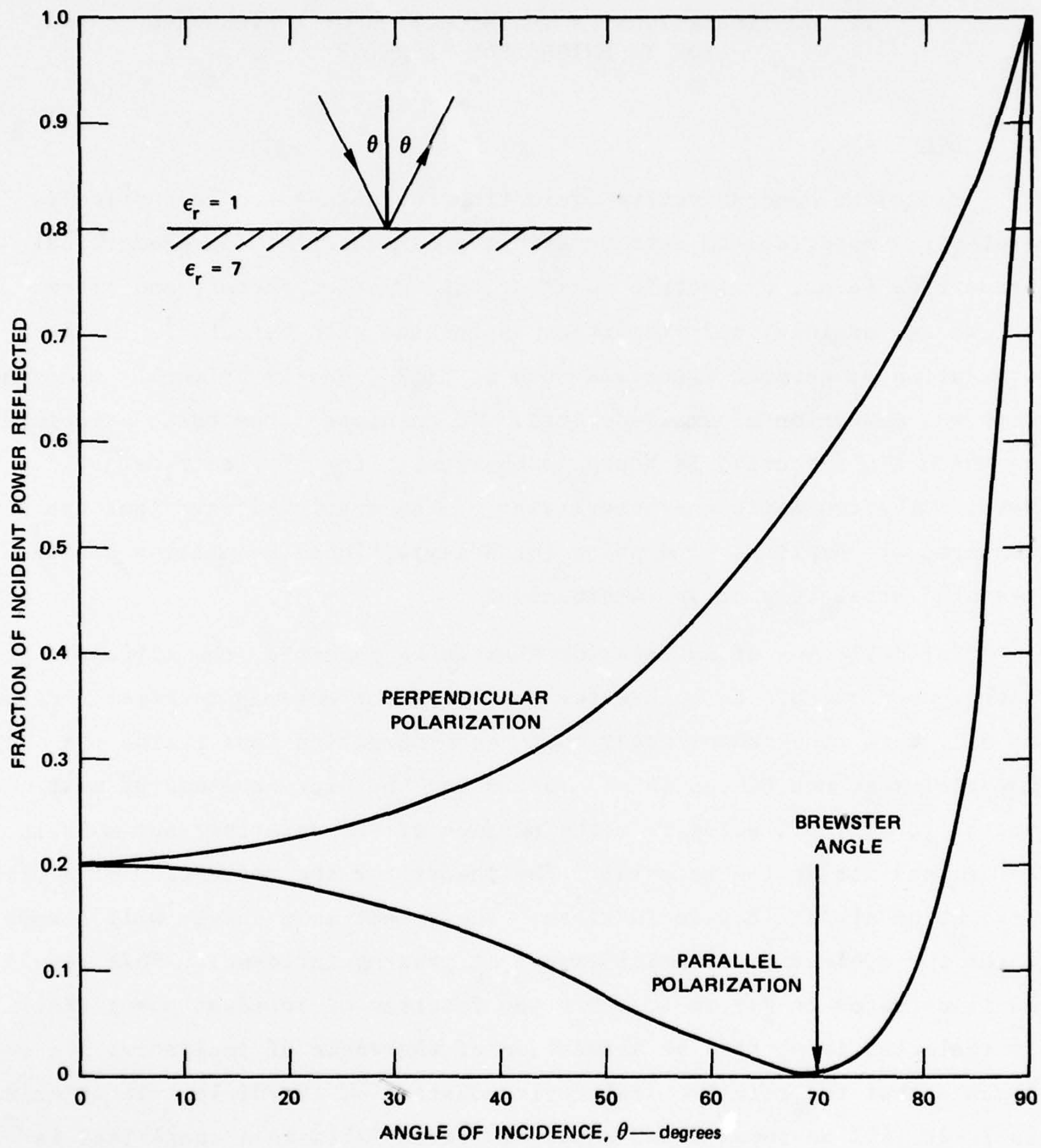

FIGURE 1 REFLECTION AT AN AIR/DIELECTRIC INTERFACE

plane of incidence that is between 0° and 90°, the polarization of the reflected wave will be rotated. For parallel polarization there is an angle of incidence where the reflected wave is zero; this angle is called the Brewster angle. Use of the Brewster angle will maximize the transmission of energy through a plane, parallel-sided dielectric plate. However, it is often simplest in practice to choose normal incidence--in this case Figure 1 shows that about 20% of the incident power will be reflected.

After the microwave energy has entered the dielectric material, it will propagate through the material until it meets a defect or a dielectric/air interface. Both perturbed and unperturbed waves will usually be partially reflected and partially transmitted when they reach a dielectric/air interface. A major exception to this rule, however, occurs when the angle of incidence of the wave at the interface exceeds a certain critical angle. In this case the wave is totally reflected and may become trapped in the material, similar to the situation in a waveguide. This condition can occur if the defect scatters energy over a wide range of angles, or if the geometry of the dielectric/air interface varies in an appropriate manner.

The behavior of the reflection of a plane wave at a plane dielectric/air interface is illustrated in Figure 2. The relative dielectric constants are the same as those used in Figure 1. It should be noted that the critical angle is fairly small in this case--namely, about 22°.

Since there is always some reflection at a dielectric/air interface (except under Brewster conditions), in general there will be standing waves inside the dielectric material. These standing waves will be particularly enhanced if the dielectric specimen is a plate with plane, parallel sides. The presence of standing waves will have a strong effect on the scattering from a defect. For example, suppose the defect is one that only interacts with electric field. If the defect is located where the electric field in the standing wave is minimum, the scattering will be much less than if the defect were located at a position of maximum electric field. Hence, since the positions of the

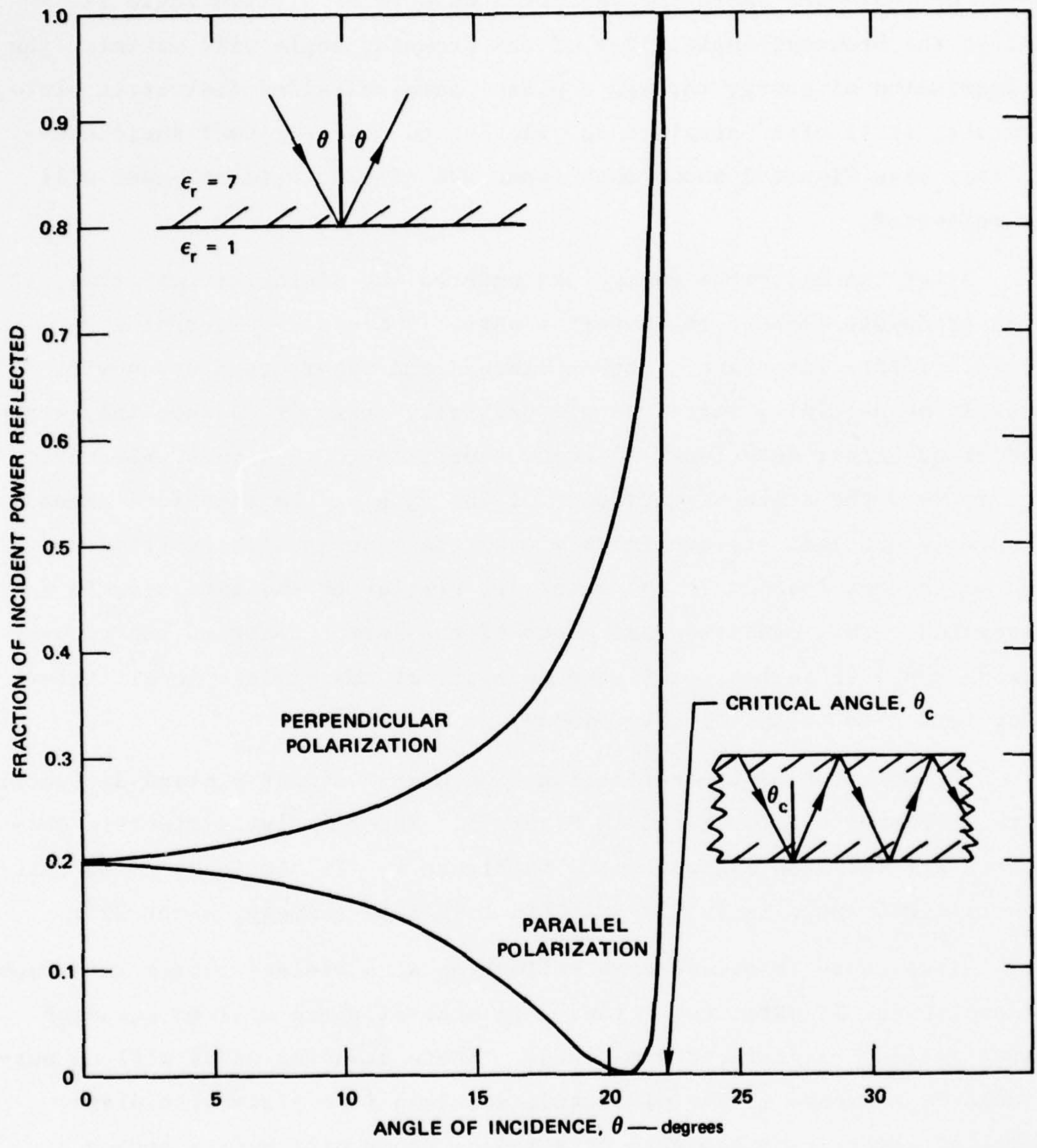

FIGURE 2 REFLECTION AT A DIELECTRIC/AIR INTERFACE

maxima and minima in a standing wave vary with frequency, the scattering from a defect will exhibit a related frequency dependence that may mask any defect-related frequency dependence in the scattering.

Scattering measurements are usually classified according to the arrangement of the transmitting and receiving antennas, and according to the operating frequency. There are three basic antenna arrangements: backscatter-monostatic, backscatter-bistatic, and forward-scatter-bistatic. These three arrangements are shown schematically in Figure 3. In the latter two of these arrangements the transmitting and receiving antennas can be either copolarized or cross-polarized.

The horns depicted in Figure 3 represent <u>any</u> kind of appropriate antenna (transducer). Microwave antennas for NDE applications can be characterized as either predominantly radiating or predominantly non-radiating. An example of the radiating type would be a horn or open-ended waveguide. A small aperture in the side of a waveguide or resonant cavity is an example of a sensor that radiates very little. In this case a defect must be close to the aperture so that interaction can take place between the defect and the reactive near fields around the aperture.

B. Sensitivity

In microwave NDE (as in ultrasonics), sensitivity (the ability to detect a defect) depends mainly on two factors: (1) the amount of scattering engendered by the defect, and (2) the ability of the detection technique to separate the desired scattered wave from undesired scattered waves. Regarding the latter factor, one is concerned with both large and small spurious scattered waves--i.e., one strives for high contrast and low background clutter, respectively. Electronic noise is also a factor in determining sensitivity, but is usually less important than clutter.

In general, the theoretical determination of the scattering from an arbitrary shape and type of defect is a difficult problem requiring computer analysis.[8] However, if it is assumed that the defects can be approximated as either metal or dielectric spheres, some rather simple

(a) MONOSTATIC BACKSCATTER

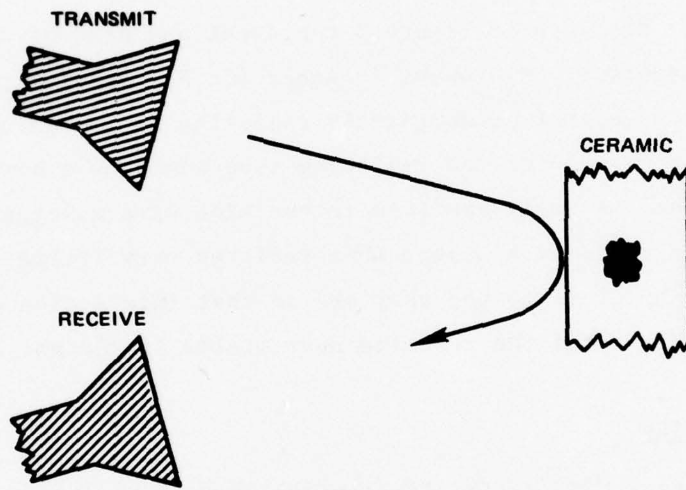

(b) BISTATIC BACKSCATTER

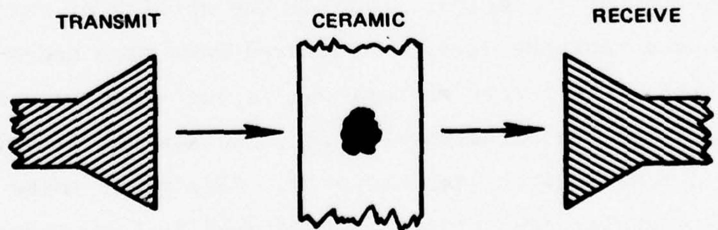

(c) BISTATIC FORWARD SCATTER

SA-5594-10

FIGURE 3 SCATTERING CONFIGURATIONS

formulas can be used when the wavelength of the electromagnetic radiation is much larger than the sphere radius (Rayleigh region). The Rayleigh criterion is

$$\frac{2\pi a}{\lambda} < 0.4 \tag{1}$$

where λ is the wavelength in the dielectric medium and a is the radius of the sphere. For example, assume that the frequency is 100 GHz and that the dielectric constant of the ceramic is 7.5 (Si_3N_4). Then, from Eq. (1),

$$a < 70\ \mu m \tag{2}$$

in the Rayleigh region.

For a conducting sphere in the Rayleigh region the scattering cross section, σ, is given by

$$\frac{\sigma(0)}{\lambda^2} = \frac{9}{4\pi}\left(\frac{2\pi a}{\lambda}\right)^6 \tag{3}$$

for backscattering, and

$$\frac{\sigma(\pi)}{\lambda^2} = \frac{1}{4\pi}\left(\frac{2\pi a}{\lambda}\right)^6 \tag{4}$$

for forward scattering. It can be seen from Eqs. (3) and (4) that backscattering is about an order of magnitude stronger than forward scattering. The factor of σ/λ^2 may be interpreted as the fraction of the total incident power that would be scattered if the total incident power were confined to an area of λ^2. Assuming $2\pi a/\lambda = 0.4$, one finds that $\sigma(0)/\lambda^2 = 3 \times 10^{-3}$, a relatively small number.

An expression similar to Eqs. (3) and (4) describes the scattering from a low-loss dielectric sphere in the Rayleigh region:[9]

$$\frac{\sigma}{\lambda^2} = \frac{1}{\pi}\left(\frac{\epsilon_r - 1}{\epsilon_r + 2}\right)^2 \left(\frac{2\pi a}{\lambda}\right)^6 \qquad (5)$$

where ϵ_r is the dielectric constant of the sphere relative to the surrounding medium. For example, for a spherical void in Si_3N_4, $\epsilon_r = 1/7.5$. This example shows that both high- and low-density defects in Si_3N_4 should produce a similar effect on the illuminating electromagnetic wave.

The defects of most interest in the NDE of ceramics have maximum dimensions between 25 and 125 μm. Equation (2) shows that scattering from such defects is of the Rayleigh type even for a frequency of 100 GHz. Thus it can be concluded that a major consideration in the microwave NDE of ceramics will be the detection of relatively small signals.

If the defect is larger than that considered above, or if the frequency is higher, interference between the scattering from different parts of the defect can occur. This situation is called resonance scattering, and increases in scattering cross section of 1 to 2 orders of magnitude over that existing at the upper end of the Rayleigh region are often observed under these conditions. Hence, operation at frequencies higher than 100 GHz may prove advantageous if the scattering from surface irregularities and grain boundaries is not too large.

If the transmit and receive antennas are co-polarized, all of the configurations shown in Figure 3 (with the possible exception of the 90° bistatic arrangement) suffer from poor contrast; that is, the small scattered signal is buried in a large specularly reflected or transmitted signal. Thus, one is forced to use a "bridge" technique to improve contrast.*

---

*The use of side-scattering would seem to be an obvious choice for the purpose of improving contrast. However, in practice, there can be side scattering from the boundaries of the test object that is of the same order of magnitude as the side-scattering from the defect. This situation makes it difficult to identify a bona fide defect. In addition, there can be nulls in the side-scattering pattern that could cause a defect to be overlooked.

There are many different kinds of bridge techniques, and, in turn, these techniques depend on whether amplitude or phase is to be measured. One simple kind of bridge would be one where a portion of the transmitted signal with the proper amplitude and phase is fed directly to the receiver so that the signal received in the absence of a defect is canceled. Another technique uses mode conversion--e.g., the detector can be made to be responsive only to a wave whose polarization is orthogonal to that of the incident wave.[10] A third technique imparts a modulation to the wave scattered by a defect[11] by appropriately vibrating or rotating the sample being inspected. The modulated wave can then be separated from any large unmodulated scattered waves that are also received by using appropriate filtering.

The use of a feed-forward canceller is not very practical at high microwave frequencies because of the sensitivity of the null condition to the position of the specular scatterer. In this case it is difficult to maintain a null as the ceramic part is scanned in front of the antennas, particularly if the part has nonplanar surfaces.

Of the remaining two contrast-improving techniques, it is simplest to implement the mode-conversion technique by using separate receiving and transmitting antennas and orienting them with their polarizations orthogonal to one another. Although the monostatic-backscatter scheme shown in Figure 3(a) appears attractive because only one sensor is required for both illumination and detection, this advantage is offset slightly by the circuit complexity required to separate the orthogonal transmitting and receiving modes. Therefore, the bistatic-forward-scatter scheme shown in Figure 3(c) (using cross-polarized antennas) was used for most of the experimental work during this program. Although scatterers with certain geometrical symmetries will not couple orthogonal modes, there is very little probability that these symmetries will occur for real defects in ceramics.

The above discussion has implicitly assumed the use of continuous-wave (CW) measurements. For the NDE of relatively thin ceramic parts (a few wavelengths thick or less), there is no advantage to be gained from

the use of pulsed measurements (or, equivalently, wideband swept-frequency measurements). Normally, pulsed measurements would be used to separate reflections (in the time domain) from various scattering centers along the direction of propagation (called ranging in radar parlance). However, the shortest practical pulse duration that can be produced and radiated results in a spatial extent for the pulse of the order of 10 wavelengths in the ceramic material. Thus, for a part that is only a few wavelengths thick, ranging cannot be accomplished.

C. Spatial Resolution

There are two different aspects to be considered under the heading of spatial resolution. One aspect is concerned with one's ability to locate a defect relative to some reference location. This is called "global" resolution. The other aspect is concerned with one's ability to differentiate between two closely spaced defects. This is called "local" resolution. Both of these aspects can be important.

As discussed previously, for thin ceramic parts microwave NDE does not provide any spatial resolution of either type in the nominal direction of propagation of the illuminating wave. In the scanning plane (defined as a plane containing all the positions of a reference point on the sample that are occupied as the sample undergoes rectilinear translation), spatial resolution is determined by the active areas of the transmitting and receiving antennas. At distances sufficiently far removed from the test piece, the "active" area is essentially determined by the far-field beamwidth of the radiating antenna.

A simple microwave antenna such as a horn must have an aperture that is several wavelengths on a side in order to minimize spreading of the beam. The beamwidths associated with this kind of antenna result in a local spatial resolution in the scanning plane that is much too gross for the ceramics application.*

---

*In principle, a "synthetic array" technique could be used to improve resolution along the line of scan. In this technique, the amplitude and phase of the scattered waves received at a number of successive sample points along the scan line are stored and then the data are processed by computer to form a high-resolution image. This technique works fine in a radar application, but probably could not be used in the special geometries associated with ceramics NDE.

The best spatial resolution using a far-field antenna is obtained by incorporating a lens into a microwave horn.[12] Such a lens can be fabricated from polystyrene, and produces a 3-dB spot size having a diameter approximately equal to one free-space wavelength at the operating frequency. Focal lengths of such lenses are typically 10 wavelengths. For reference, it is useful to keep in mind that the free-space wavelength at 100 GHz is equal to 3 mm.

An alternative approach, and one that can yield comparable magnitudes of resolution, is to move the test piece into the near fields of the antennas. In this case the active area of the antenna is simply equal to the effective aperture of the antenna. The size of this effective aperture depends on the nature of the fringing fields around the aperture and the distance between the aperture plane and the scanning plane.

One of the simplest types of antenna is an open-ended waveguide. Typical aperture dimensions for such an antenna at 100 GHz are about 0.4 by 0.8 free-space wavelengths, or 1.25 by 2.5 mm. Higher resolutions can be obtained by reducing the aperture size[11] (i.e., by using an electrically small antenna). However, this approach results in a trade-off between sensitivity and resolution. Overall sensitivity is lost when the aperture size is reduced because less of the total available power "leaks" through the aperture (unless there is compensation by appropriate impedance matching). In addition, an electrically small antenna radiates relatively very little energy, and the near fields associated with it fall off very rapidly with distance from the antenna. Thus, when using such an antenna, one runs the risk of not detecting a defect inside the ceramic material.

An important advantage of obtaining good local spatial resolution is the minimization of spurious scattering caused by variations in the gross geometry of the ceramic part. Signals due to slow variations in geometry can be removed by filtering, but a small active sensor-area is the only solution if one wishes to inspect a part very close to a sharp change in boundary surface (such as an edge).

Because of the long delivery time and expense involved, it was not practical to obtain microwave lenses for use during this program. Hence, open-ended waveguides were used as sensors. In general, the achievable spatial resolution in the scanning plane of such a system depended on the thickness of the ceramic part that was inspected. For example, if the scanning plane is located 4 mm from the aperture plane of the open-ended waveguide, the 3-dB beamwidth[13] in the scanning plane at 100 GHz is about 14 mm in the E plane, and 6 mm in the H plane.* This resolution was adequate for studying the widely spaced defects in the 0.25-inch-thick seeded plates that were examined during this program.

---

*In antenna parlance, the E-plane is a plane containing the transverse E-field and the direction of propagation. Similarly, the H-plane contains the transverse H-field and the direction of propagation.

III DIELECTRIC PROPERTIES OF Si_3N_4 AT MICROWAVE FREQUENCIES

Detection of flaws within Si_3N_4 depends on the losses in the material being small and there being some difference between the electrical properties of the Si_3N_4 and those of the flaw. Since there is very little information available on the electrical properties of bulk Si_3N_4 at high microwave frequencies, SRI undertook a small task to measure these properties.

The dielectric properties of Si_3N_4 depend on the type of process used for fabrication (reaction sintering, hot pressing, etc.). Published data taken at 10 GHz on samples of Si_3N_4 produced by different processes show values of relative dielectric constant ranging between 5.5 and 9.3, and loss tangents ranging between 0.001 and 0.15.[14] Hence, measurements were conducted during this program using both reaction-sintered and hot-pressed material (Norton NC132); the emphasis, however, was placed on the latter material.

Two different measurement techniques were used for determining relative dielectric constant and dissipation loss. For frequencies up to 18 GHz, the reflection and transmission properties of a sample inside a coaxial holder were measured using a Hewlett Packard Model 8542B automatic network analyzer. For higher frequencies, free-space measurements of the reflection and transmission for a plane, parallel-sided plate were used.

In the automatic-network-analyzer system an SRI-generated computer program accepts the measured complex reflection and transmission data and calculates several material parameters.[15] These parameters are:

- The complex air/material-interface E-field reflection and the complex propagation constant within the material that would exist as if the material was semi-infinitely thick with only one air/material interface.

- The complex relative dielectric constant, ϵ_r (permittivity).
- The complex relative permeability, μ_r.*
- The loss tangent.
- The attenuation constant of the material, in dB/cm.

The measurement procedure in this case requires that the sample be in the form of an annulus. This sample is mounted in a precision 50-ohm, 7-mm beadless-airline coaxial transmission line (Maury Microwave Model 2653-1250). This holder permits measurements to be made over a very wide frequency range and eliminates the measurement errors associated with the small reflections produced by the dielectric support beads in a conventional coaxial line. The diameters of the outer and inner coaxial conductors of the transmission line are 7.00 mm (0.2756 in) and 3.04 mm (0.1197 in), respectively. The samples that were measured were cut and ground to be a slip fit to the coaxial line by a local ceramics fabrication house (RW Products, Redwood City, California).

The dielectric properties of three different ceramic materials were measured using this system. The first material tested was a piece of reaction-sintered Si_3N_4 obtained from the Materials Center of SRI. The sponsor provided a second sample that was intended to be hot-pressed Si_3N_4 (Norton NC132), but which proved to be hot-pressed silicon carbide (SiC). This fact was determined from X-ray diffraction analysis. Therefore, some Norton NC132 was obtained from the SRI Materials Center, and this served as the third test material.

The SiC sample was found to have so much dissipation loss (in fact it exhibited dc conductivity) that the calculated values of ϵ_r probably have little meaning. The air/material interface reflection was high, being about 0.85 at all frequencies from 0.2 GHz to 18 GHz. The attenuation within the material was very high, ranging from about 10 dB/cm at 1 GHz, to about 70 dB/cm at 10 GHz, to about 100 dB/cm at 18 GHz. Thus, microwaves would not be suitable for probing very far into this material.

---

*For Si_3N_4, the permeability was assumed to be the same as for free space. However, the computer program is general enough to be able to handle magnetic materials.

The fraction of reflected incident power and the attenuation for infinitely thick samples of reaction-sintered and hot-pressed Si_3N_4 are plotted as functions of frequency in Figure 4. These results were derived from measurements using a sample of finite thickness. The reaction-sintered material appears to be less dense than the hot-pressed material because the power reflected from the reaction-sintered material is less than for the hot-pressed material. The corresponding derived values for the real part of the relative dielectric constant are:

- Hot-pressed Si_3N_4: $\epsilon_r = 7.5$ (at 8-17.5 GHz)
- Reaction-sintered Si_3N_4: $\epsilon_r = 5.7$ (at 8 GHz) to 6.0 (at 17.5 GHz).

On the other hand, the attenuation in the reaction-sintered material was higher than for the hot-pressed material. In face, the losses in the hot-pressed material were so low that the attenuation could not be measured accurately at most of the measurement frequencies. Such low losses cause the data-reduction computer program to give inaccurate results for the dielectric parameters when the sample is an integer multiple of one-half wavelength thick. One can see from Figure 4 that this situation occurs at about 13.5 GHz, where the sample is one wavelength thick (0.406 cm). Fortunately, alternate data reduction of the reflection coefficient and insertion loss of the finite sample provide accurate means for determining the reflection factor and attenuation at this frequency. The resulting calculated value for the attenuation is plotted in Figure 4, and is seen to be less than 0.2 dB/cm.

It can be concluded that, for frequencies up to 17.5 GHz, the values of reflection factor and attenuation for Si_3N_4 (either type) do not prevent the use of microwave NDE. However, one can anticipate the need to operate at higher microwave frequencies--for example, in the range 50-100 GHz--in order to obtain better resolution. Hence, some dielectric measurements were also conducted at these higher frequencies.

The approach used to determine the dielectric constant of ceramic materials at frequencies above 50 GHz is based on the fact that the reflection from a plate having flat, parallel faces is a minimum whenever the thickness of the plate is an integer multiple of one-half the

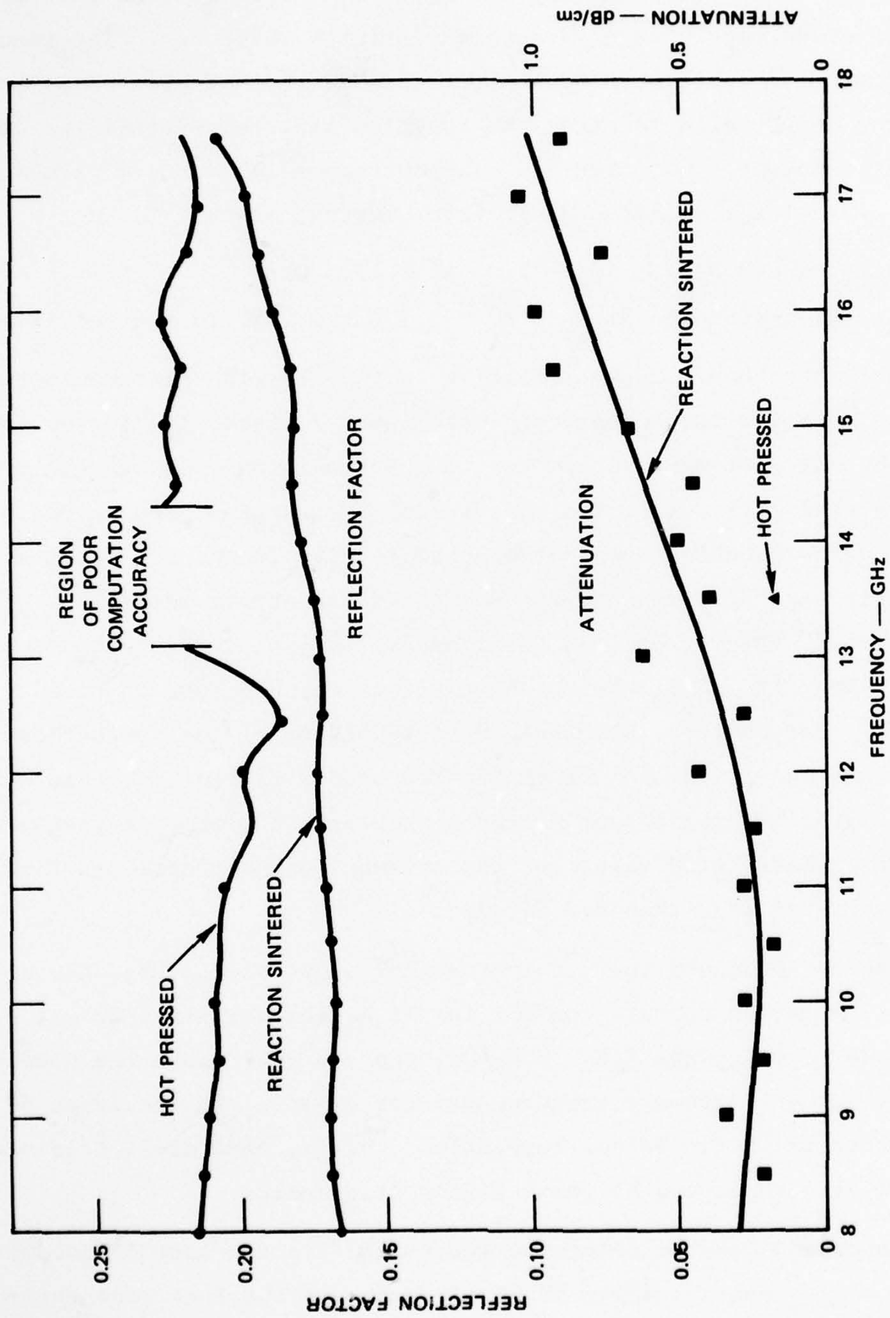

FIGURE 4 MEASURED DIELECTRIC PROPERTIES FOR Si_3N_4

wavelength in the material. If f_1 and f_2 are adjacent frequencies where reflection minima occur, the relative dielectric constant, ϵ_r, can be computed from the equation

$$\epsilon_r = [c/(f_2 - f_1)2t]^2 \quad (6)$$

where c is the velocity of light in free space and t is the thickness of the plate. For example, for a hot-pressed Si_3N_4 plate 0.635 cm thick, it was found from measurement that f_1 = 53 GHz and f_2 = 62 GHz. Substitution of these numbers into Eq. (6) gives the result ϵ_r = 6.9. This value is comparable to, but smaller than, that obtained at lower frequencies; this discrepancy could be due to experimental error.

The output-power-versus-frequency characteristic of the available 100-GHz source (backward-wave oscillator) was too erratic to permit determination of ϵ_r at 100 GHz. For the same reason only a qualitative determination of the dissipation loss in the material at this frequency could be obtained from the plate transmission and reflection measurements. It was clear from these measurements, however, that the dissipation loss in hot-pressed Si_3N_4 is relatively small even at 100 GHz, and so it was concluded that such losses do not constitute a major limitation for the microwave NDE of this material at these frequencies.

IV EXPERIMENTAL DETECTION AND LOCATION OF DEFECTS IN Si_3N_4

A. General

In accordance with the general considerations discussed in Section II, the scattering measurements conducted during this program utilized open-ended waveguides as transmitting and receiving antennas. Usually, both of the waveguide apertures were placed as close to the surface of the material under test as possible in order to obtain the best local spatial resolution. In scanning, the waveguides were fixed and the sample was moved. Normal incidence was always used; however, the position and polarization of the receiving antenna were varied. The evolution of these measurements was such that frequencies below 18 GHz (K-band) were used first, then frequencies near 50 GHz (V-band), and finally frequencies near 100 GHz (W-band). The following subsections present the results obtained for these three frequency ranges.

B. K-Band Measurements

The first sample of hot-pressed Si_3N_4 to be examined during this program was a disk 4 inches in diameter and 0.3-inch thick that had been prepared by the sponsor. When received, the surface of this disk was in the rough, as-pressed state and initial measurements on the disk were conducted without further surface finishing. Later in the program, the surfaces of the disk were ground smooth, and additional measurements on this sample then were carried out.

An X-ray radiograph of the as-pressed Si_3N_4 disk showed that it contained a small high-density inclusion about 0.020 inch in size. Therefore, in making K-band scattering measurements on the disk, a scan line was chosen that caused the inclusion to pass directly under the illuminating open-ended waveguide that was positioned about 0.020 to 0.030 inch above the surface. In these measurements the open-ended waveguides were aligned so that the electric-field vectors for the dominant TE_{10} mode in

PRECEDING PAGE NOT FILMED
BLANK

each waveguide were parallel* (i.e., the antennas were co-polarized). The waveguides used were type WR-62, which have inside dimensions of 0.622 by 0.311 inch.

All the scattering measurements in this band were carried out using the automatic-network-analyzer system. The results of measurements conducted at 17.5 GHz are shown in Figure 5. Both 90° side-scattering and forward and backscattering were measured. The topmost curve in the figure shows the return loss as a function of probe position along the scan line. Return loss is the ratio of the power reflected by a perfect reflector to the actual power reflected. At the center of the disk, it can be seen that about 25% of the incident power is reflected. This result is in agreement with the measured value of reflection factor for an infinitely thick sample given in Figure 4. From the reflection data, it appears that the edges of the sample can be located to within ± 0.1 inch. However, there was no obvious indication of the inclusion in the reflection data.

The middle curve in Figure 5 shows the results for 90° side-scattering. In this case, the distance between the centers of the open-ended waveguides was about 2.8 inches. The curve shows that the measured transmission loss for side-scattering exhibits variations on the order of 10 dB, and that there is a loss peak near the center of the disk. This peak might be associated with the presence of the inclusion, but, if so, the indicated location of the inclusion is significantly in error. A more probable explanation is that the central peak (as well as those near the edges of the disk) is associated with scattering from the edges of the disk. Since the distance between illuminating and receiving antennas is about four free-space wavelengths at the measurement frequency, and the disk is about six wavelengths in diameter, it is likely that waves scattered by the edges of the disk and traveling via different paths to the receiver will interfere with one another to produce significant variations in the received signal.

---

*It was soon found that co-polarized measurements were always accompanied by high clutter levels. Subsequent measurements all used crossed polarization.

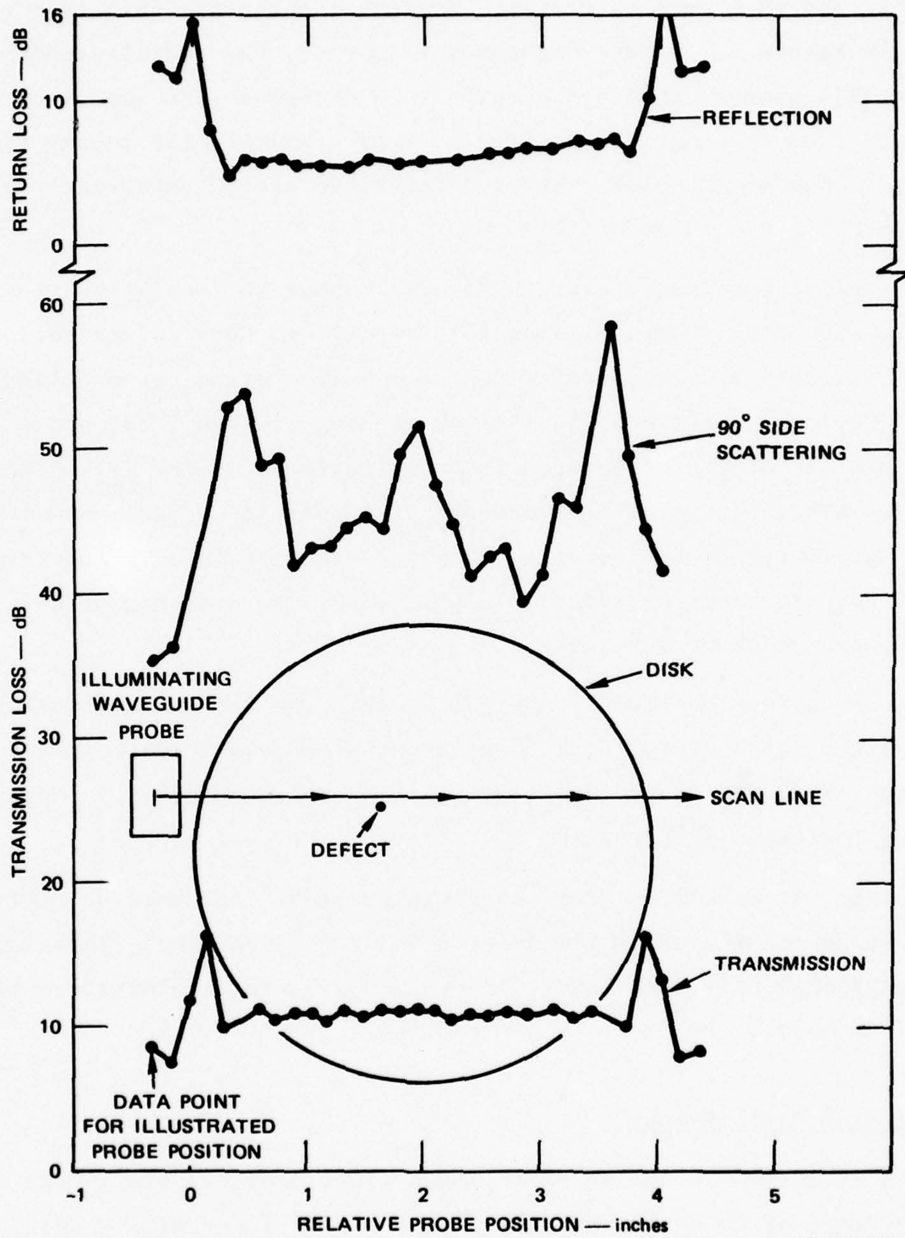

FIGURE 5 MEASURED SCATTERING AS A FUNCTION OF PROBE POSITION. Hot-pressed Si_3N_4; as-pressed surface; 17.5 GHz.

This conjecture is given further credibility by the fact that large variations in received signal are also observed when the probe position is fixed and frequency is varied. Typical results for this case are shown in Figure 6. As the frequency is varied, the radial standing waves in the disk change, and this results in a change in the amount of energy radiated from the edge of the disk. It is primarily the energy radiated from the edge of the disk that is detected in the 90° side-scattering experiment.

Finally, the lower curve in Figure 5 shows the measured transmission loss for the disk. Transmission loss is defined here as the ratio of power available from the source to the power received (also called insertion loss). Out of the nominal 11 dB of transmission loss, about 1.25 dB is the result of the reflection from the surfaces of the disk. Based on the previous attenuation measurements discussed in connection with Figure 4, it can be concluded that most of the remaining transmission loss is due to beam-spreading. In this case, the distance between the waveguides was about 0.5 inch.

Also, it can be seen from Figure 5 that the transmission measurement locates the edges of the disk to within the achievable disk-positioning accuracy of ±0.020 inch. However, again there is no obvious indication that an inclusion is present.

Hence, it was clear from these measurements that more sensitivity would be needed if such small defects are to be detected. This conclusion suggested that the higher frequencies and cross-polarized antennas should be used.

C. V-Band Measurements

As discussed in the previous subsection, measurements in the frequency range of 15 to 17 GHz showed that higher frequencies would be needed to obtain adequate sensitivity and resolution for detecting and locating the defects of interest in Si_3N_4. Accordingly, a transmission test setup was implemented for operation in the frequency range 40 to 60 GHz. The block diagram for this experimental arrangement is shown in Figure 7.

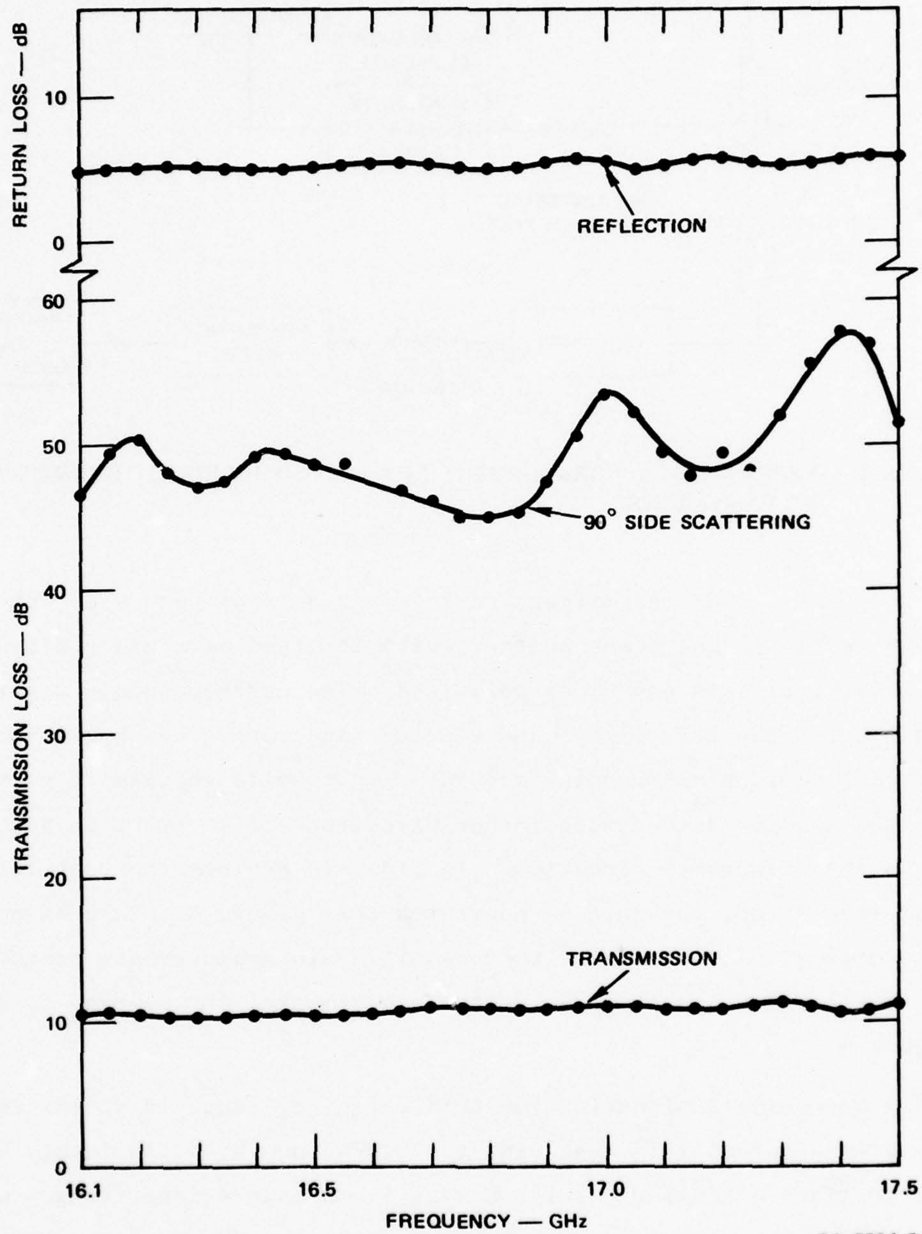

FIGURE 6 MEASURED SCATTERING AS A FUNCTION OF FREQUENCY FOR HOT-PRESSED Si_3N_4 DISK. Probe positioned at center of disk along scan line shown in Figure 5.

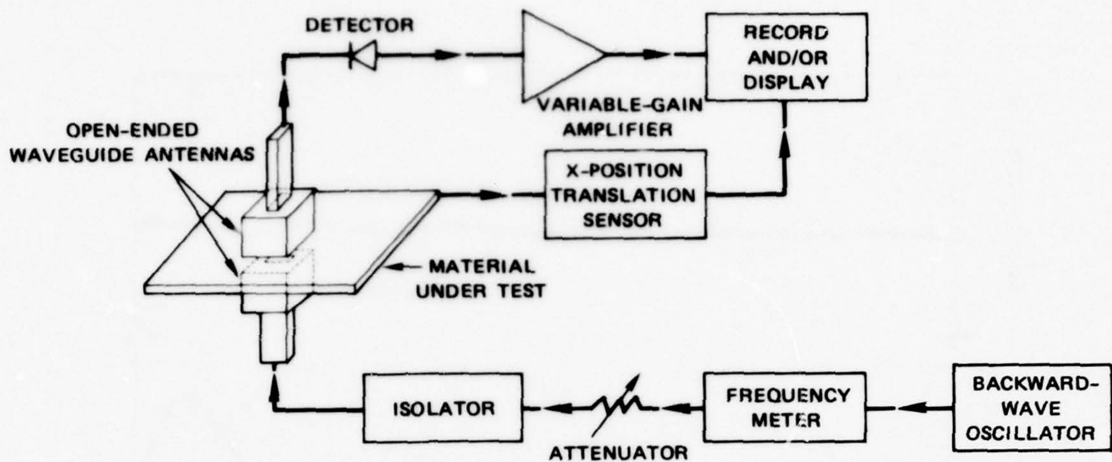

FIGURE 7 EXPERIMENTAL ARRANGEMENT FOR CROSS-POLARIZED TRANSMISSION MEASUREMENTS

Physically, the transmitter and receiver antenna apertures were placed directly opposite one another, with the feed waveguides aligned along a vertical axis and cross-polarized. The ceramic sample was then placed between the transmitter and receiver and moved in a horizontal plane. The horizontal scanning mechanism that holds the sample provided a continuous motor-driven scan in one direction and movement in precise steps in the orthogonal direction. In order to achieve the best local spatial resolution, the antenna apertures were placed as close as possible to the surfaces of the sample, thus resulting in measurements of the near-field scattering. A photograph of the experimental arrangement is shown in Figure 8.

The waveguide designation for this frequency range is WR-19; the inside dimensions of this waveguide are 0.094 inch by 0.188 inch. Special rugged sections of this waveguide having 1.125-inch-square flanges were constructed. These sections were used next to the sample for enhanced rigidity of the system, and with the expectation that effects due to the fringing fields near the edges of the waveguide would be reduced because of the wide flanges.

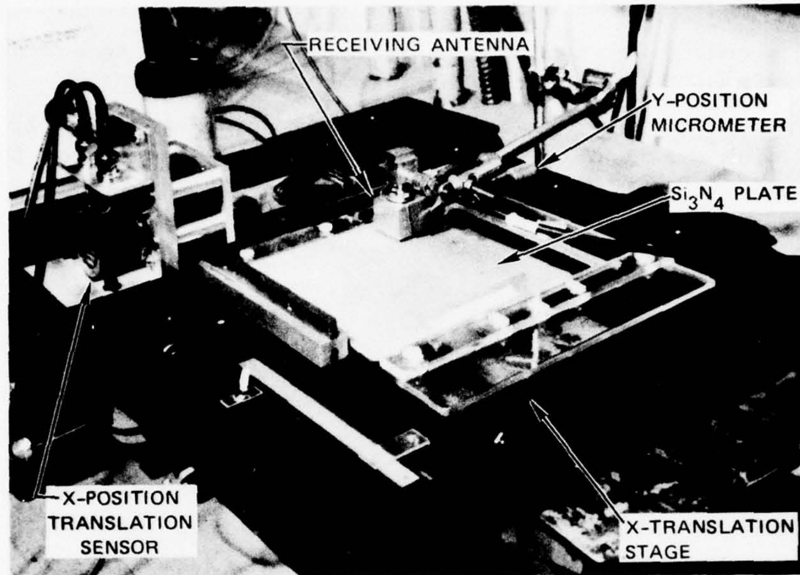

TOP VIEW

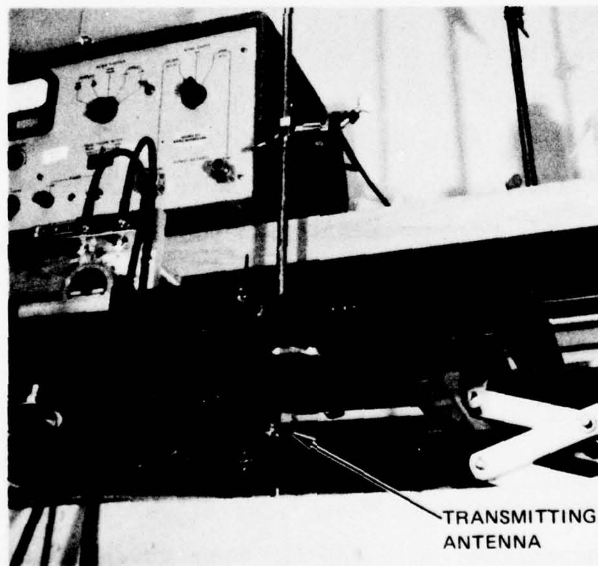

BOTTOM VIEW

SA-5594-12

FIGURE 8 PHOTOGRAPHS OF EXPERIMENTAL ARRANGEMENT FOR CROSS-POLARIZED TRANSMISSION MEASUREMENTS

Three different types of transmitter antenna were tried:

(1) An open-ended waveguide with a 1.125-inch square flange.

(2) A standard waveguide attached to a 1.125-inch square plate having a 0.040-inch-diameter pinhole in its center.

(3) A TE_{102} cavity formed by taking the arrangement of (2) and adding a second iris at an appropriate distance from the first.

Comments on the utility of these transmitter schemes will be made in conjunction with relevant data as they are presented later in this subsection.

About the time of the implementation of the V-band test set-up, a billet* of hot-pressed Si_3N_4 (NC132) seeded with inclusions was received from the sponsor. This billet was used in the ensuing measurements. The type and intended locations of the intentional defects in the billet are shown in Figure 9. For reference purposes, each flaw has been identified in the figure by specifying its row and column. For instance, the 0.005-inch-diameter tungsten carbide flaw closest to the bottom of the plate is denoted Flaw (6.1).

The actual positions of some of the flaws were determined by the sponsor using ultrasonic C-scan imaging, and the results are shown in Figure 10. By comparing this figure with Figure 9, one notes that some of the flaws have wandered from their intended positions, and that some unintentional flaws of undetermined type are present. About half of the intended 0.005-inch-diameter defects were not visible in the copy of the ultrasonic C-scan that was provided with the billet.

Figure 11 presents some typical results that were obtained using the microwave-transmission C-scan† arrangement. Figure 11(a) shows the area of the seeded billet that was covered in the scan. This area included two rows of the 0.020-inch-diameter flaws of all four types. The transmitter antenna in this case was the open waveguide with a 1.125-inch-square flange, and the frequency was 56.4 GHz. The receiving antenna

---

*Designated Billet E307103897, Plate No. 3.

†The term "C-scan" is commonly used to describe the imaging of material variations in the scanning plane.

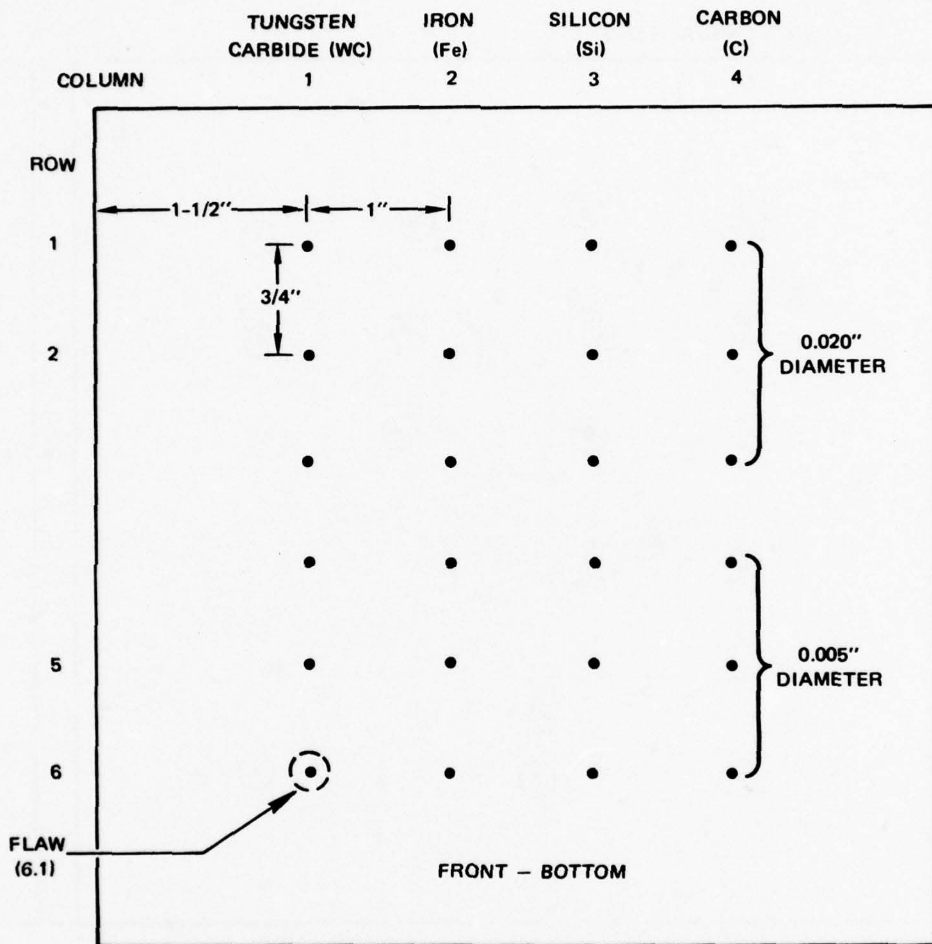

FIGURE 9 INTENDED FLAW LOCATIONS FOR SEEDED Si_3N_4 BILLET

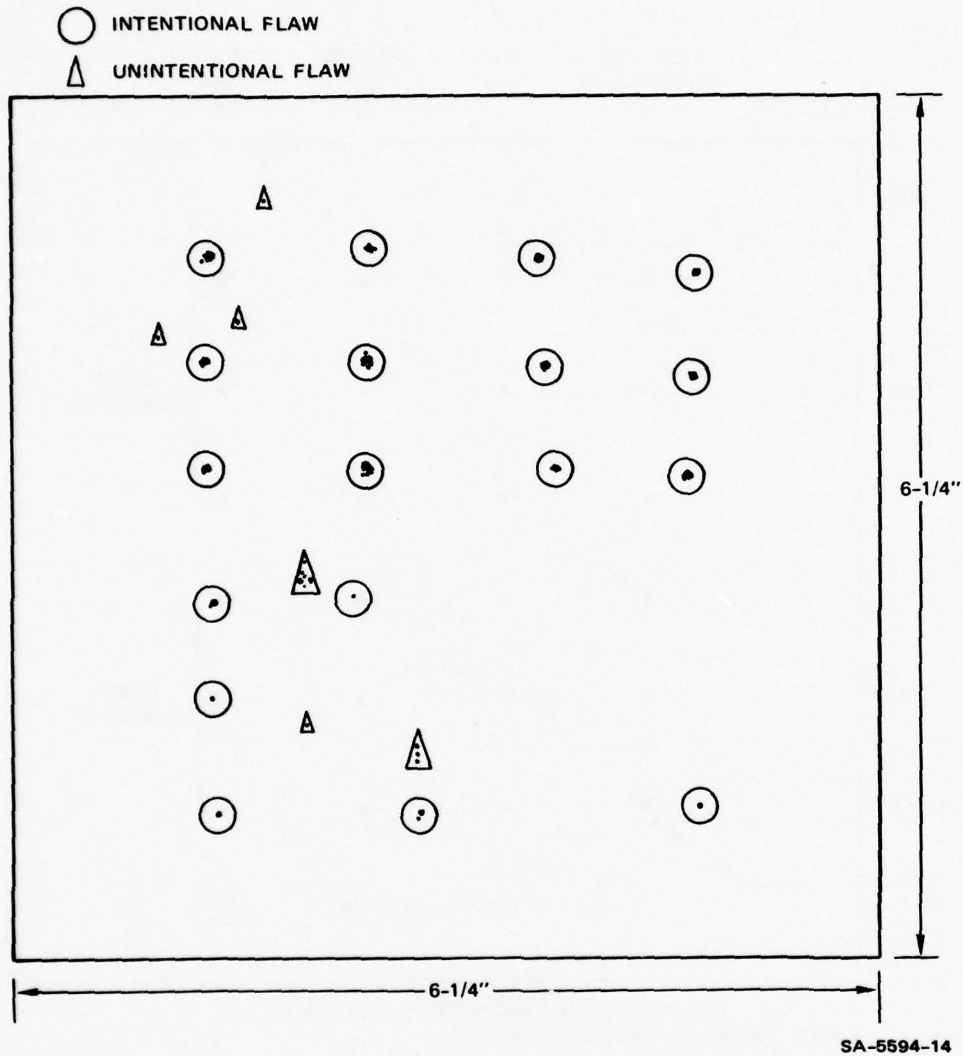

FIGURE 10 ULTRASONIC C-SCAN MAP SHOWING ACTUAL POSITIONS OF FLAWS. 25 MHz; focused transducer. Some flaws were not detected.

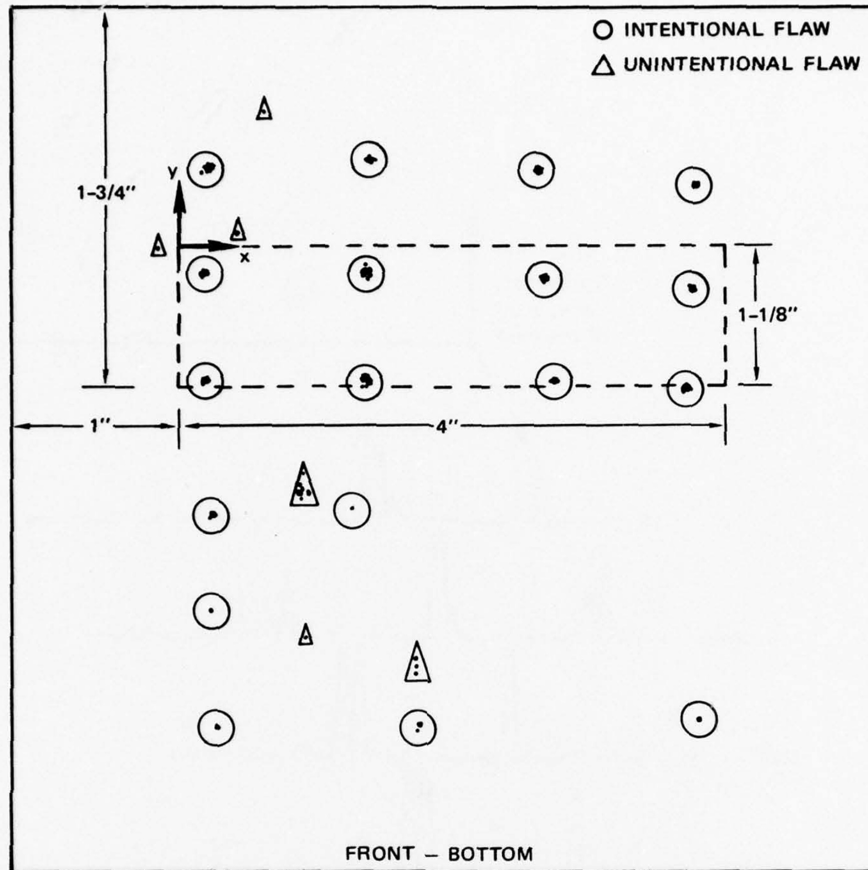

(a) ULTRASONIC C-SCAN MAP OF FLAWS SHOWING AREA COVERED BY MICROWAVE C-SCAN

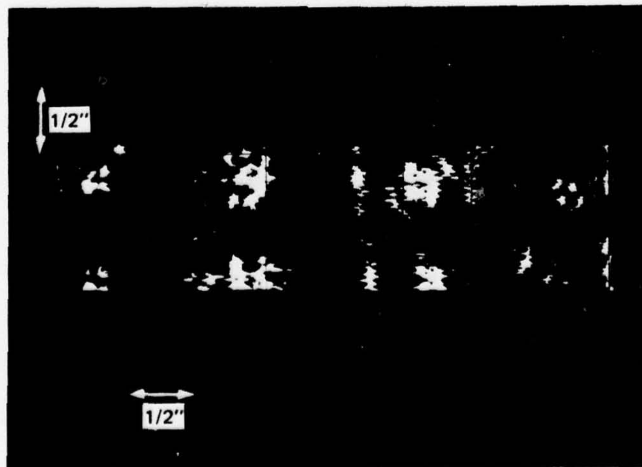

(b) MICROWAVE C-SCAN OF FLAWS (displayed on storage oscilloscope using intensity modulation)

SA-5594-15

FIGURE 11 TYPICAL RESULTS OBTAINED USING MICROWAVE (V-band) C-SCAN MAPPING

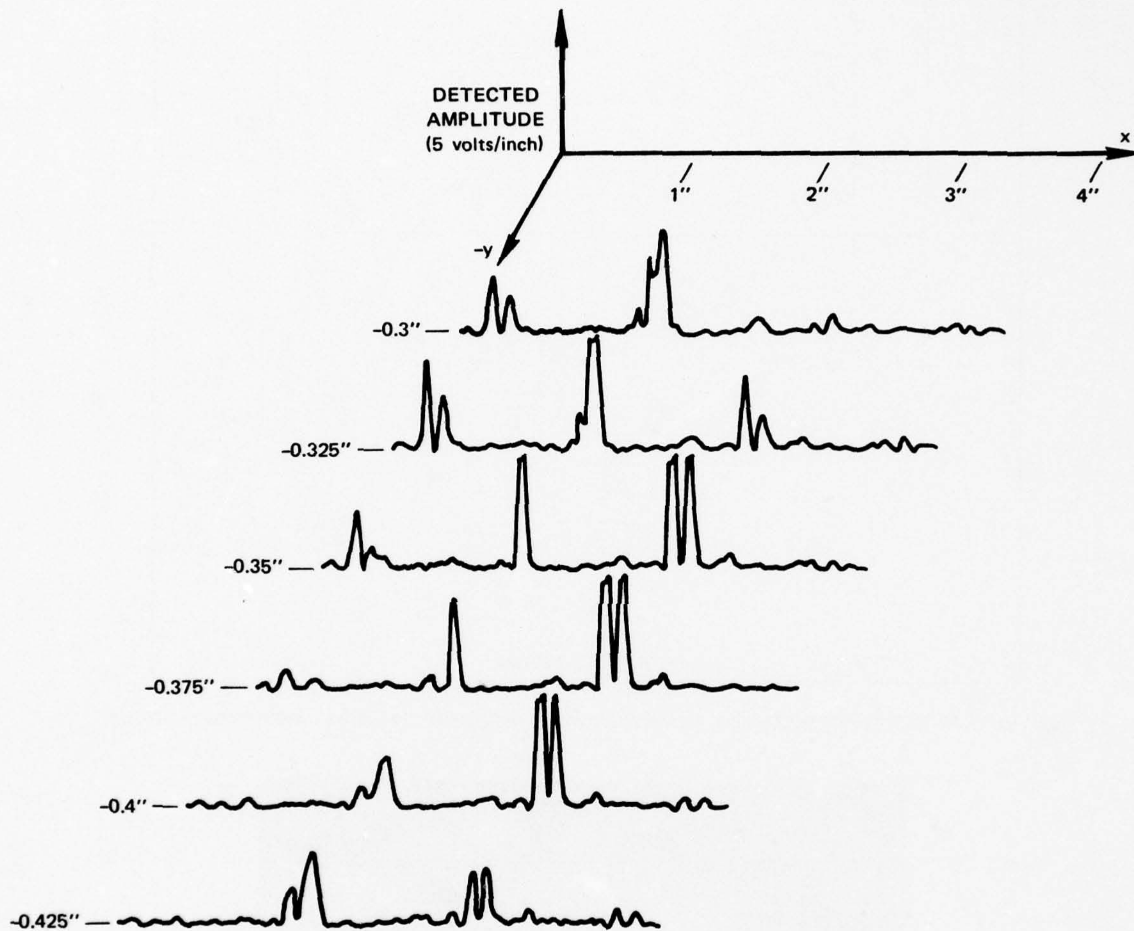

(c) EXAMPLES OF THE AMPLITUDE VARIATION OF THE SIGNAL DETECTED IN THE SCANNED AREA

SA-5594-16

FIGURE 11 (Concluded)

(identical to the transmitting antenna) was rotated by 90° so as to receive only the cross-polarized scattered signal. The microwave C-scan map shown in Figure 11(b) was obtained by modulating the intensity of the display of a storage oscilloscope with the received scattered signal. All eight of the intended defects in the scanned area were detected, and apparently some unintended flaws were detected as well. For example, some spurious signals are evident on both sides of flaw (2.3) (silicon). The local spatial resolution in this display is determined by the size of the waveguide (i.e., the operating frequency), and the combination of signal amplitude and threshold setting on the storage oscilloscope.

Figure 11(c) shows a plan-position plot of detected amplitude versus position for a few scans in the coverage area. The transverse increment between scans was 0.025 inch. It can be seen that a multiple-peaked response from a single defect is quite common. In general, the shape of this response is determined both by the geometrical shape of the defect and by interference effects due to multiple scattering. Multiple scattering can occur when there is scattering from the boundaries of the test piece. The resulting interference pattern is analogous to the speckle pattern that is observed when an object is illuminated by coherent light. The use of focused transmitting and receiving antennas would reduce this effect. In cases where multiple scattering can be made negligible, the shape of the detected response obtained in the microwave C-scan might be usable for flaw identification or shape determination.

Microwave C-scans were also taken in areas of the plate that contained the smaller (0.005-inch-diameter) defects. Typical results for this case are shown in Figure 12. Two scans are shown for comparison: one for the 0.020-inch-diameter flaws and one for the 0.005-inch-diameter flaws. In both cases the open-waveguide transmitter was used and the frequency was 56.3 GHz. Both the small tungsten carbide and iron defects give large signals. On the other hand, the small silicon and carbon particles could not be detected at this frequency.

As was mentioned earlier, three different types of transmitter antennas were actually tried in the transmission measurements. A comparison

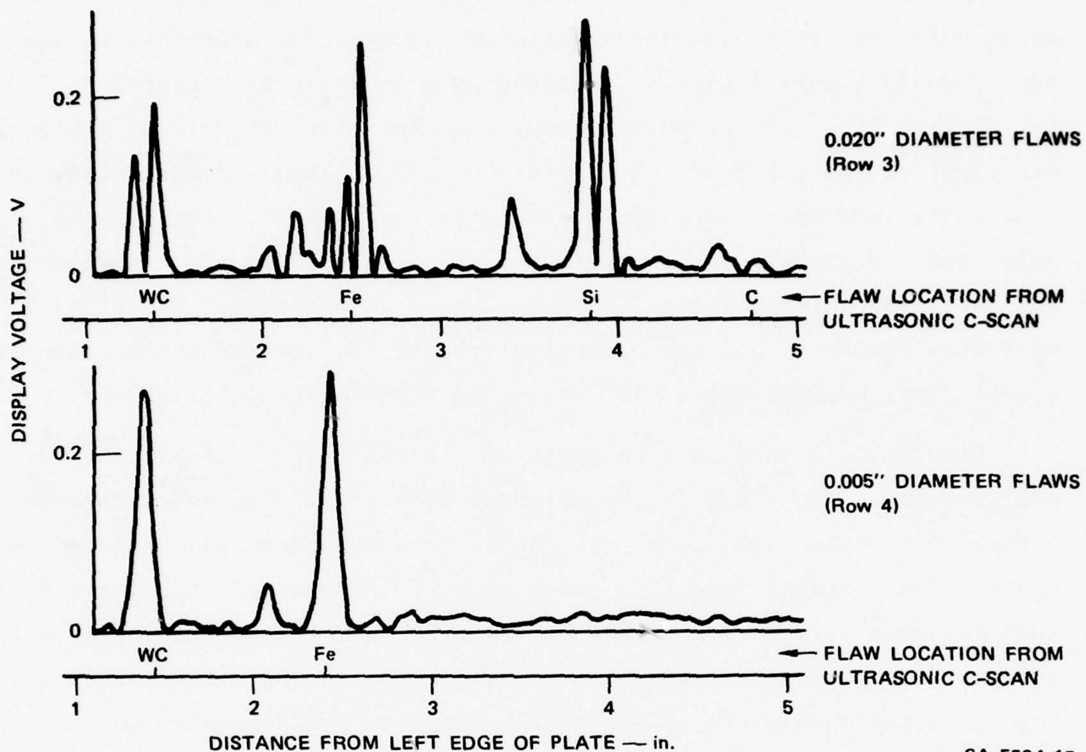

FIGURE 12 TYPICAL MICROWAVE (V-band) C-SCAN AMPLITUDE PRESENTATIONS FOR LARGE AND SMALL INCLUSIONS. Open-waveguide transmitter.

between the typical responses obtained using the three different techniques is shown in Figure 13. In each case, the transmitted power and receiver gain were adjusted to optimize the signal-to-noise ratio and dynamic range, so only a qualitative comparison is possible. In general, the open-waveguide antenna gave the best results because it produced the largest signal level. The spatial resolution obtained using the open-waveguide transmitter was about the same as for the pinhole and resonant-cavity transmitters. This is because the beam spread from a pinhole is larger than from the corresponding waveguide, so the beam size at the position of the defect (about 1/8 inch from the transmitter) is about the same in all cases (approximately 0.25 inch).

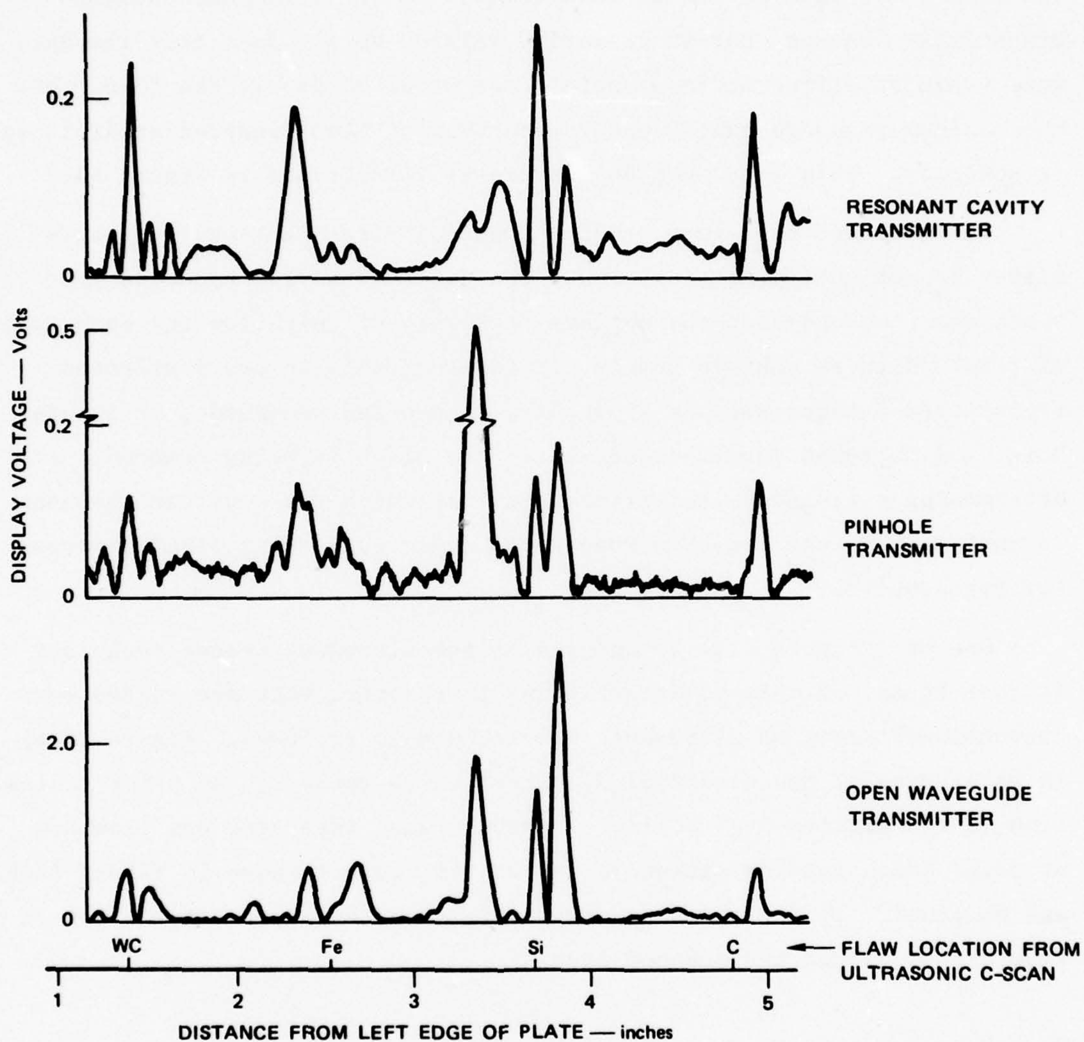

FIGURE 13 TYPICAL V-BAND RESPONSES FOR DIFFERENT ILLUMINATION TECHNIQUES. Scans across row 1 of flaw locations shown in Figure 9.

It will be noted in Figure 13 that the same flaws produce different relative magnitudes of response for the different transmitter schemes. The reason for this is not so much related to the difference between transmitter schemes, but is primarily related to the fact that the data were taken at different frequencies. In other words, it was found that the maximum response exhibited by each type of flaw occurred at different frequencies. This frequency dependence is illustrated in Figure 14.

It is clear, therefore, that the use of a resonant-cavity transmitter is not good practice because the cavity's narrow bandwidth prevents one from choosing the optimum frequency of operation for each type of flaw. With an unknown sample, it is preferable to use a wideband transmitter antenna such as a pinhole, open-ended waveguide, or focused horn, and to sweep the frequency while the plate is being scanned. After determining a frequency (or frequencies) at which the receiver response is most marked, one can then repeat the scans using this single frequency (or frequencies).

One of the potential advantages of the microwave C-scan technique is that it may be able to detect flaws in ceramics that are missed when conventional X-ray or ultrasonic NDE techniques are used. Figure 15(a) shows an area of the seeded Si_3N_4 billet where there was no prior indication of the existence of a flaw. However, when this area was examined at 58.67 GHz using the microwave C-scan, the result shown in Figure 15(b) was obtained. It is very clear from this measurement that some type of flaw exists within the scanned area.

D. W-Band Measurements

Based on the encouraging results obtained at 40 to 60 GHz, it was decided to implement a cross-polarized microwave transmission C-scan system for the frequency range 75 to 110 GHz, since the necessary equipment had become available during the latter part of the program. It was expected that these higher frequencies would provide improved sensitivity and resolution for defect detection and localization in Si_3N_4, and this expectation was borne out by the experiments.

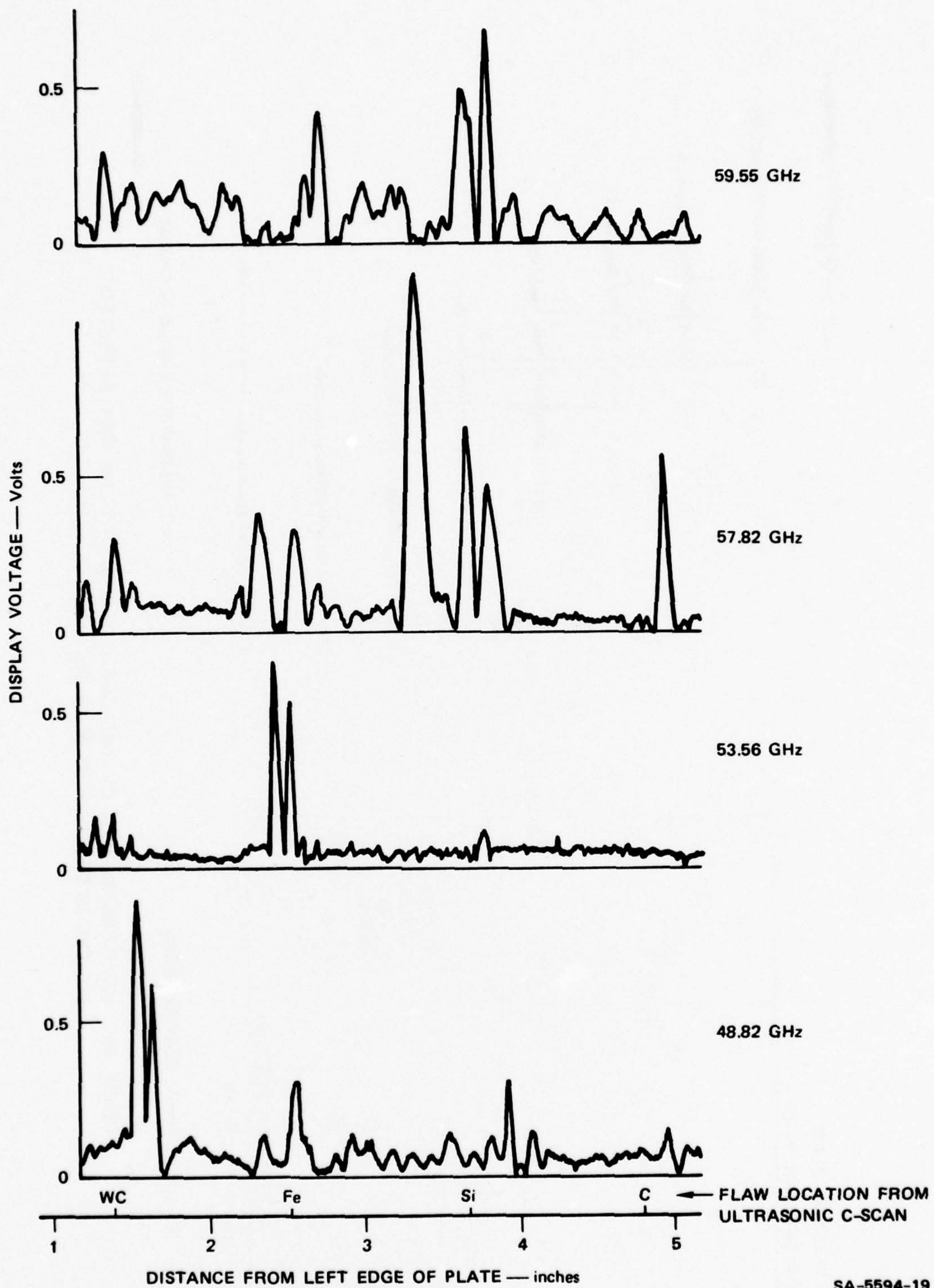

FIGURE 14 AN ILLUSTRATION OF THE EFFECT OF FREQUENCY ON DETECTED RESPONSE USING A PINHOLE TRANSMITTER. Scans across row 1 of flaw locations shown in Figure 9.

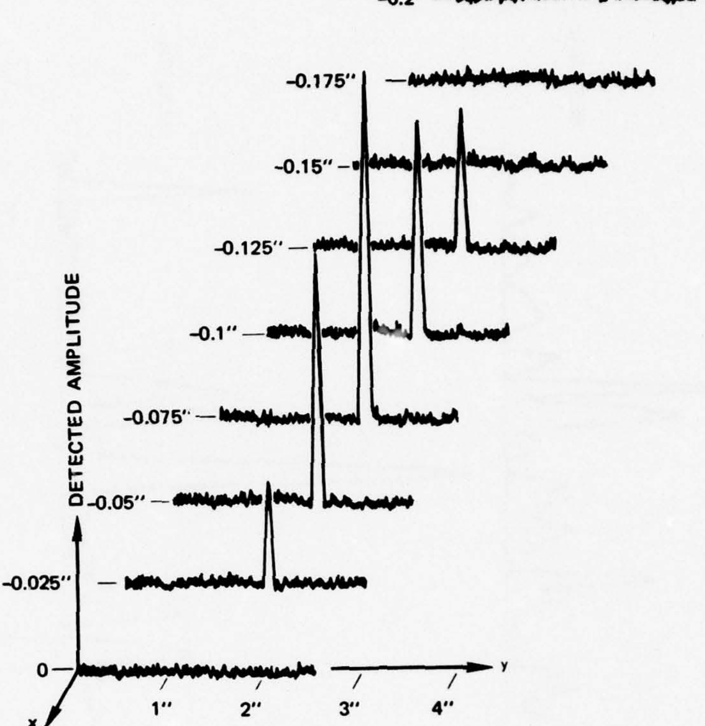

(a) LOCATION OF SCANNED AREA

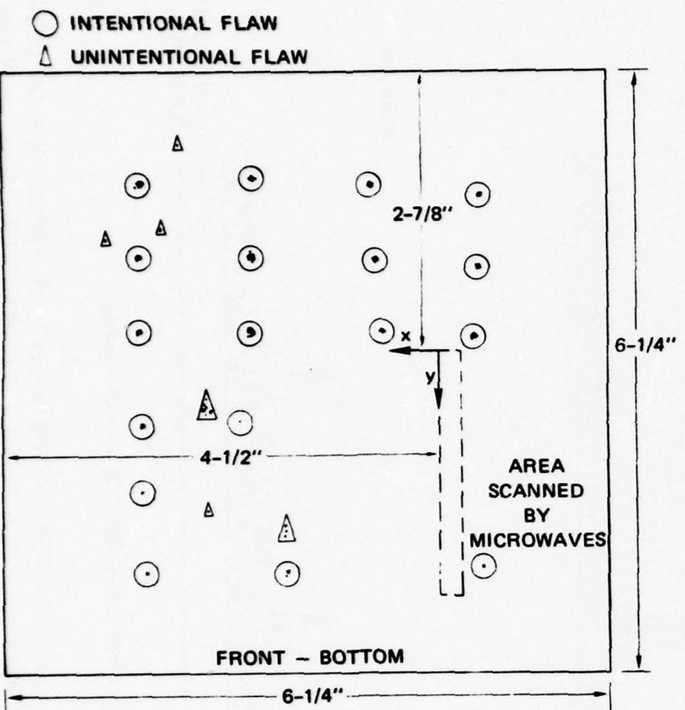

(b) MICROWAVE C-SCAN RESPONSE

SA-5594-20

FIGURE 15 AN ILLUSTRATION OF THE DETECTION OF A FLAW NOT DETECTED BY THE ULTRASONIC C-SCAN TECHNIQUE

In earlier experiments, the detected signals were recorded and displayed continuously using either a storage oscilloscope or an X-Y recorder. For these high-frequency W-band measurements, however, the detected signal was sampled at a set of points in the scan area, and then recorded using an FM tape recorder. These data were then subsequently digitized and processed with a computer to produce a display.

Figure 16 shows a block diagram of the data-acquisition system. In this system, acquisition was initiated by pressing a start button just before the scan was begun. The accumulator-comparator combination generates a series of sampling (clock) pulses as the scan proceeds. Each sampling pulse corresponds to a particular point in space on the scan line; this correspondence is not affected by the scanning speed. Data acquisition is terminated when the accumulator overflows, which corresponds to a predetermined threshold voltage--say, 10 V. The number of sample points is determined by the scan increment. Typically, about 250 points were sampled over a 4-inch scan length, giving a spatial sampling resolution of 0.016 inch. This degree of spatial resolution was more than adequate for even the W-band measurements, since the beamwidth in the defect plane of the open-ended-waveguide antenna was at least 10 times larger than the scan increment.

Broad-flange, open-ended waveguides were again used to achieve broadband operation. These waveguides were type WR-10, which have inside dimensions of 0.050 by 0.100 inch. Since the backward-wave oscillator is capable of being swept over a wide frequency range, it was possible to determine the best operating frequency in the neighborhood of 100 GHz for each type of inclusion. Typical frequency responses for four important types of inclusions are shown in Figure 17. The nominal diameter of these inclusions was 0.020 inch. It can be seen from the figure that there are significant variations in these frequency responses, and this fact may prove useful for flaw identification. However, as was mentioned before, these frequency responses are determined in part by the reflections from the surfaces of the ceramic plate containing the inclusions, and thus it may be difficult to separate the flaw-dependent information from these responses.

FIGURE 16 SYSTEM FOR THE ACQUISITION OF SAMPLED DATA

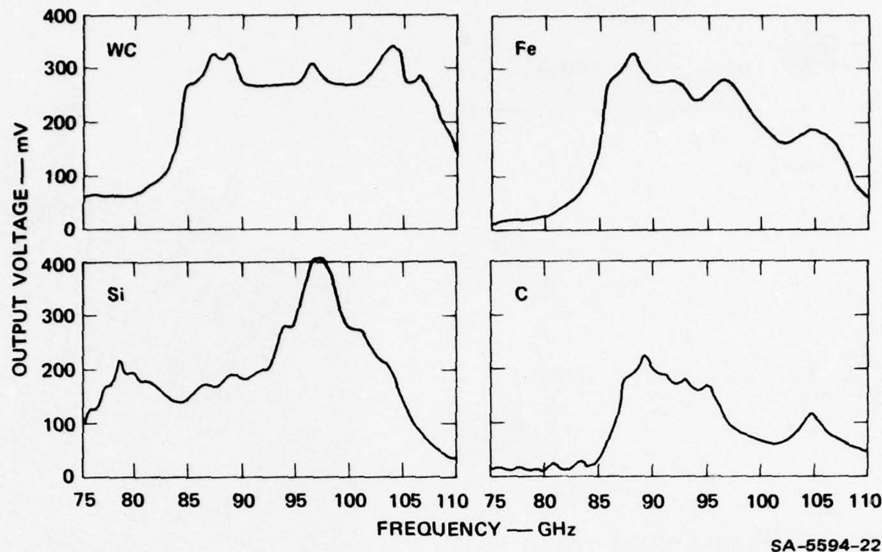

FIGURE 17 FREQUENCY DEPENDENCE OF THE CROSS-POLARIZED FORWARD SCATTERING FROM FOUR TYPES OF INCLUSIONS IN A HOT-PRESSED Si_3N_4 PLATE – BILLET E307103897.

Several different samples of Si_3N_4 containing seeded inclusions and voids were examined in W-band using the cross-polarized transmission technique. Figure 18 shows a C-scan of a portion of the hot-pressed plate described in Figures 9 and 10 that contains 0.020-inch- and 0.005-inch-diameter inclusions of WC, Fe, Si, and C. Figure 18(a) shows the area covered by the scan and the intended flaw locations. Figure 18(b) shows the portions of the scan area that produce a scattered signal greater than an arbitrarily selected threshold value. Finally, Figure 18(c) shows the amplitude of the scattered signal as a function of position within the scan area.

Several features of this C-scan are noteworthy. First, all of the 0.020-inch-diameter flaws were detected. Iron provides the strongest signal, and is the only 0.005-inch-diameter flaw that is clearly detected in this figure (the other small flaws become more apparent if the frequency is changed). Second, X-rays show that diffusion of the iron inclusion during hot pressing produces an irregularly shaped scatterer

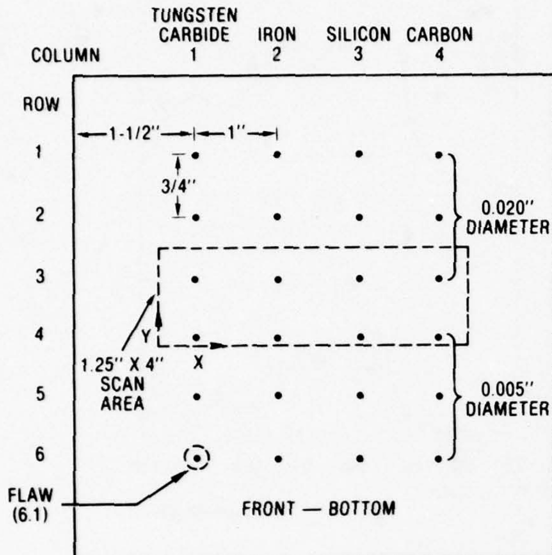

(a) Map of Intended Flaw Locations Showing Scan Area

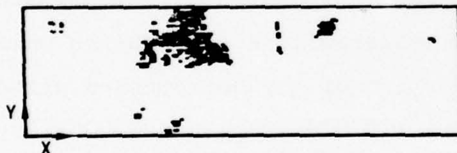

(b) Excess Signal vs. Position

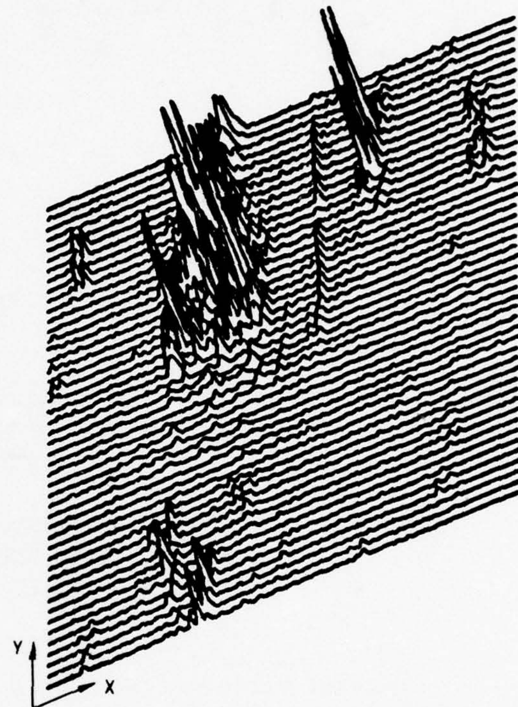

(c) Amplitude vs. Position

SA-5594-23

FIGURE 18 MICROWAVE (W-band) CROSS-POLARIZED TRANSMISSION C-SCAN OF FOUR TYPES OF INCLUSIONS IN HOT-PRESSED Si_3N_4 – BILLET E307103897. Frequency = 94 GHz.

that causes the spatial extent for this flaw to appear overly large in the microwave C-scan. Finally, it appears that a crack-like flaw is present between the 0.020-inch-diameter iron and silicon inclusions. Apparently, X-ray, ultrasonic, and dye-penetrant examination by the sponsor did not reveal the presence of such a flaw. If this flaw is indeed real, it would indicate the superior sensitivity of the microwave technique for detecting this type of flaw.

Figure 19 shows a similar microwave C-scan, but for a surface-ground, hot-pressed Si_3N_4 plate that contained different types and densities of inclusions. This plate was borrowed from AiResearch Manufacturing Company of Phoenix, Arizona. All of the 0.005-inch-diameter inclusions were detected in this scan, but, of course, the close spacing between the inclusions in this plate may have enhanced this detection.

Another scan of the same plate as in Figure 19 is presented in Figure 20, but only of the area containing the 0.001-inch-through-0.010-inch-diameter silicon inclusions. The sensitivity of the microwave technique for the detection of unreacted silicon appears to be good, and may be better for this purpose than other techniques. This feature could be important in a process-control application.

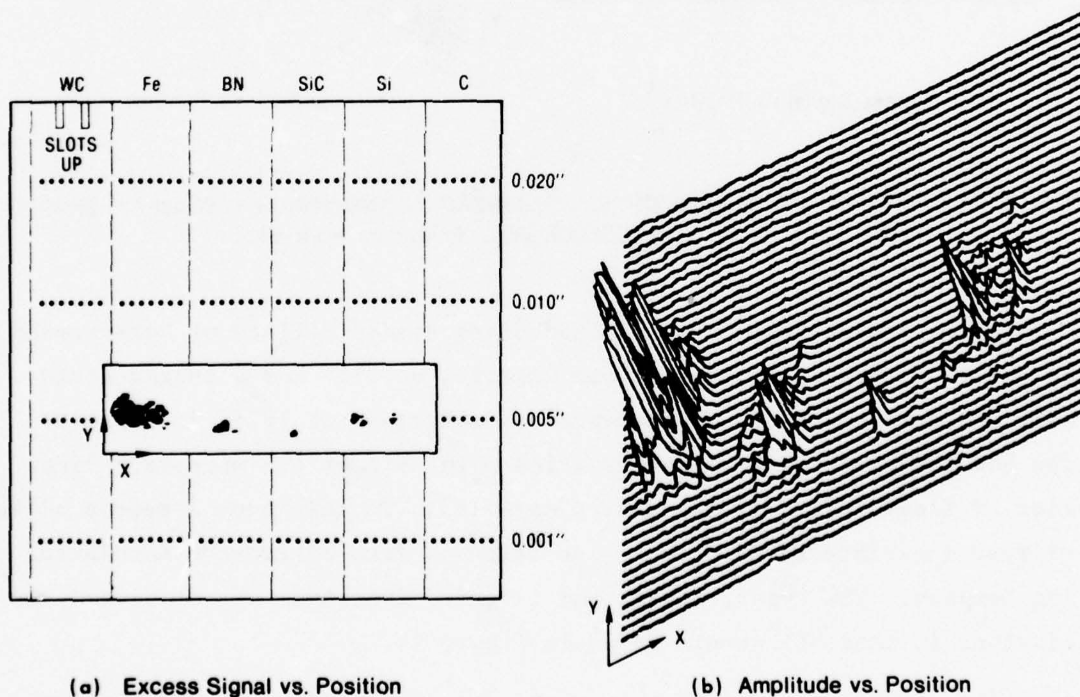

(a) Excess Signal vs. Position

(b) Amplitude vs. Position

SA-5594-24

FIGURE 19 MICROWAVE (W-band) CROSS POLARIZED TRANSMISSION C-SCAN OF FOUR TYPES OF INCLUSIONS IN HOT-PRESSED Si_3N_4 — AIRESEARCH MANUFACTURING COMPANY BILLET. Frequency = 91 GHz.

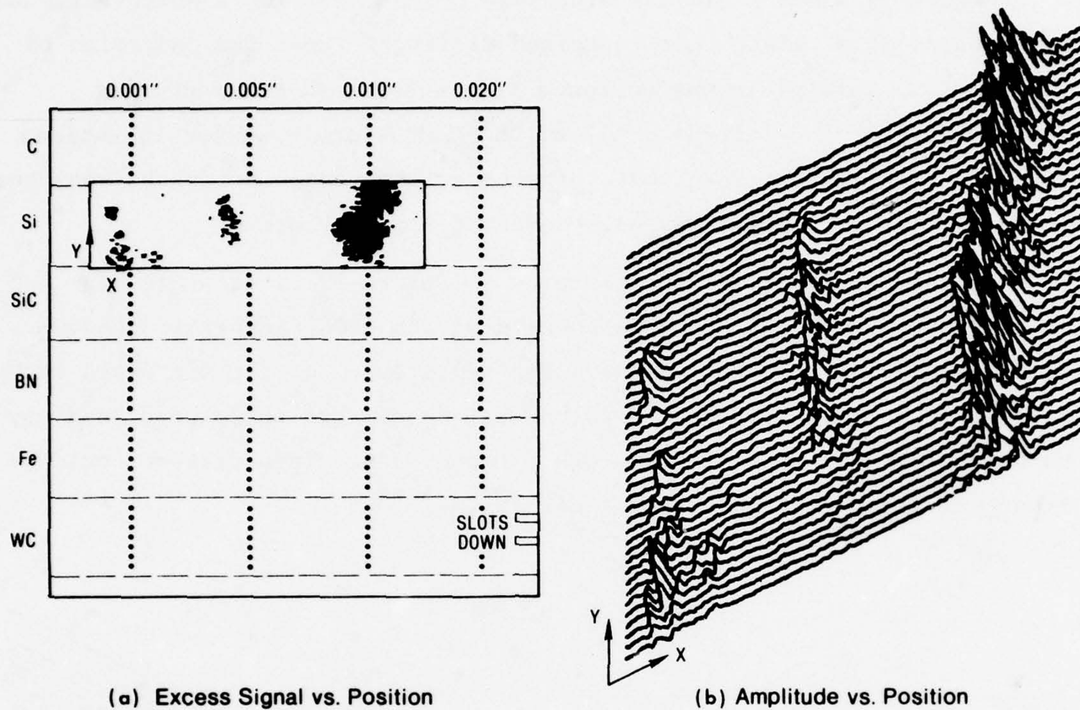

(a) Excess Signal vs. Position

(b) Amplitude vs. Position

SA-5594-25

FIGURE 20 MICROWAVE (W-band) CROSS POLARIZED TRANSMISSION C-SCAN OF SILICON INCLUSIONS IN HOT PRESSED Si_3N_4. Frequency = 98 GHz.

These results were all obtained using seeded billets of hot-pressed material. Since reaction-sintered material usually has a larger grain size and more porosity than hot-pressed material, it is of interest to see how these material characteristics might affect the microwave detection of flaws in reaction-sintered material. To this end, a seeded billet of reaction-sintered Si_3N_4 was also borrowed from AiResearch Manufacturing Company. The types, sizes, and intended locations of the seeded inclusions in this billet are shown in Figure 21.

Two different areas of this plate were examined using the microwave C-scan system. The locations of these areas are also indicated in Figure 21. Figure 22 shows the results obtained for the scan area containing the 0.020-inch- and 0.010-inch-diameter inclusions of Si and SiC. It can be seen that some of both of these two types and sizes of inclusions were

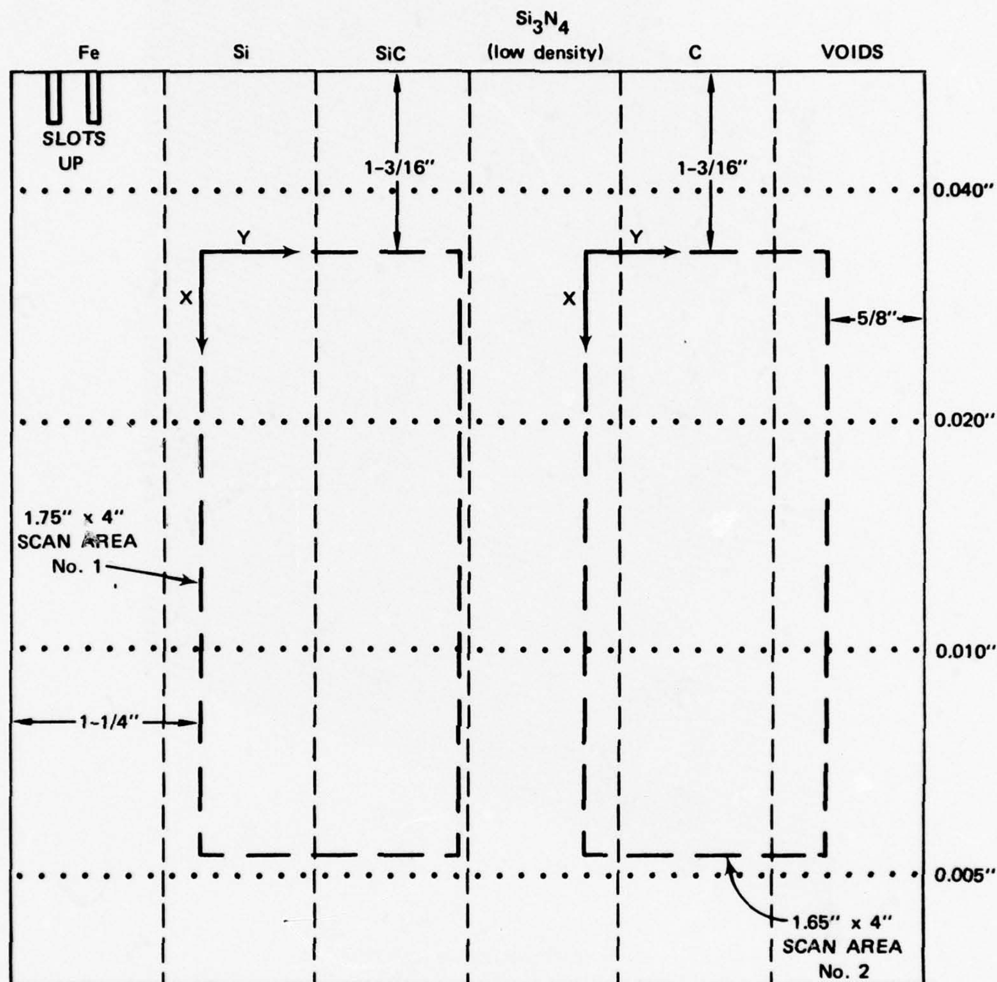

FIGURE 21 INTENDED FLAW LOCATIONS AND SCAN AREAS IN REACTION-SINTERED Si_3N_4 — AIRESEARCH MANUFACTURING COMPANY BILLET

detected. In addition, an apparent unintended flaw of some sort can also be seen. X-ray data for this plate were not available, so the existence of this unintended flaw could not be confirmed.

Figure 23 shows similar data for the scan area containing the carbon inclusions and voids. An increase in clutter level can be noticed in this figure. Generally speaking, it was found that the reaction-sintered material produced a higher clutter level than did hot-pressed material.

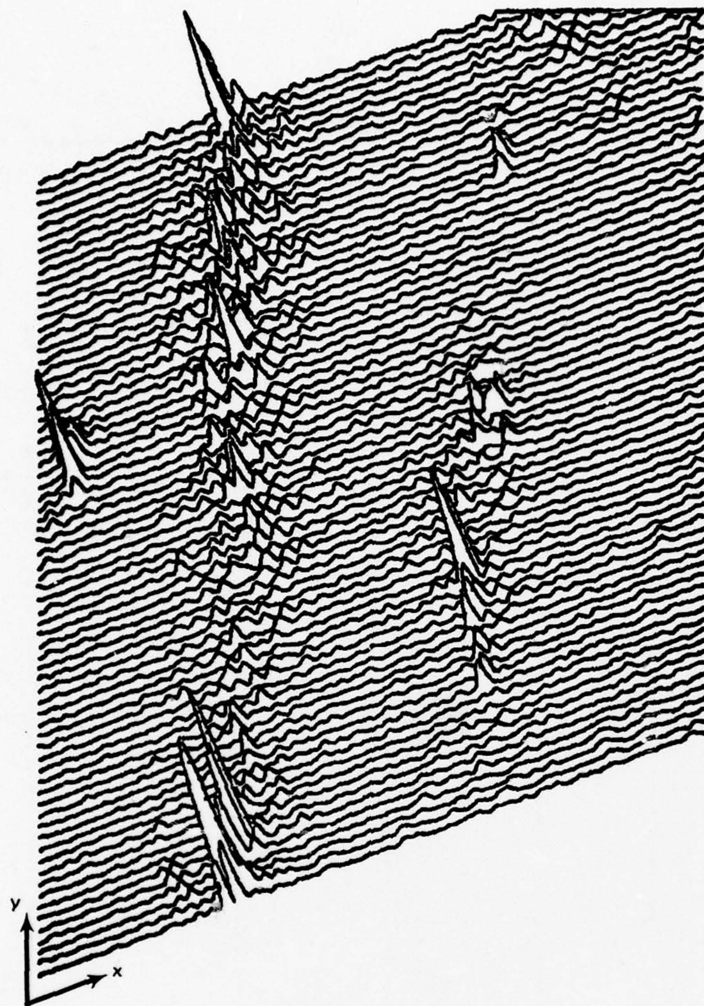

(a) AMPLITUDE vs POSITION

(b) EXCESS SIGNAL vs POSITION

SA-5594-27

FIGURE 22 MICROWAVE (W-band) CROSS-POLARIZED TRANSMISSION C-SCAN OF SCAN AREA No. 1 (Si-SiC) IN REACTION-SINTERED Si_3N_4. Frequency = 92.6 GHz.

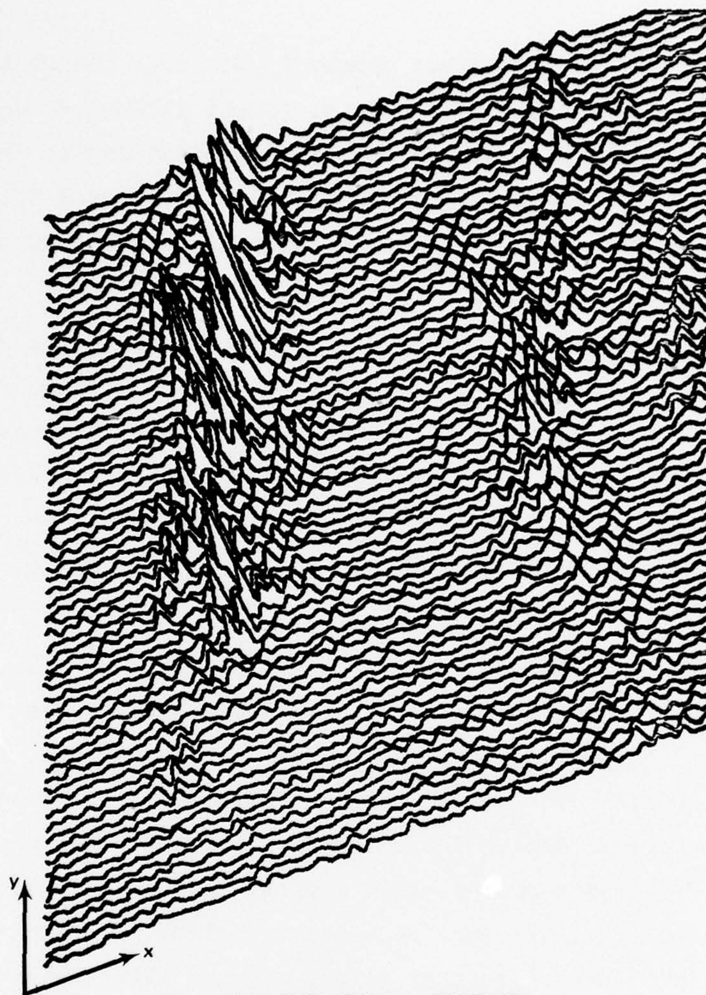

(a) AMPLITUDE vs. POSITION

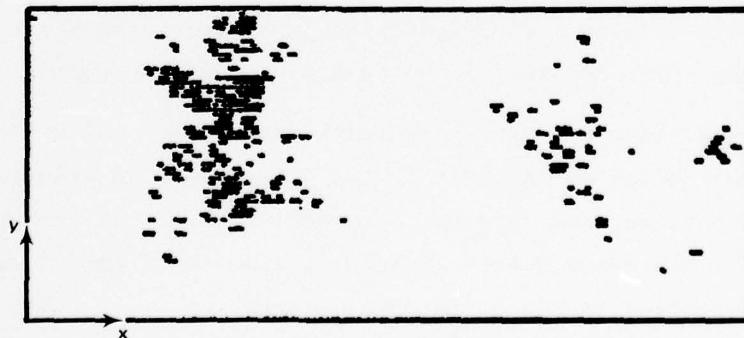

(b) EXCESS SIGNAL vs POSITION

SA-5594-28

FIGURE 23 MICROWAVE (W-band) CROSS-POLARIZED TRANSMISSION C-SCAN OF SCAN AREA No. 2 (C-voids) IN REACTION-SINTERED Si_3N_4. Frequency = 92.6 GHz.

However, the clutter level does not appear to be large enough to mask detection of 0.010-inch-diameter inclusions. Small inclusions were not examined in this billet because of mechanical limitations in the scanning system, but it is clear that inclusions having a size equal to, or less than, the grain or pore size in the material will not be distinguishable from the background.

The same conclusion holds, of course, with regard to the effect of surface roughness. During the program, a relative comparison was made of the scattering from a disk of hot-pressed Si_3N_4 having an as-pressed, grit-blasted surface, and the scattering from the same disk after surface grinding. Qualitatively, the difference in clutter level for the two surface conditions was about the same as that observed for hot-pressed and reaction-sintered material.

It appears from Figure 23 that voids as well as inclusions can be detected in Si_3N_4. In order to study this possibility in more detail, measurements were conducted on a hot-pressed, surface-ground, Si_3N_4 billet that contained seeded voids. This billet* was also supplied by the sponsor. The voids were formed in the interior of a 0.250-inch-thick Si_3N_4 plate by first drilling small holes in a 0.125-inch-thick plate, and then diffusion-bonding this plate to a second 0.125-inch-thick plate. The data shown in Figure 24 further illustrate the ability of the microwave system to detect small voids in Si_3N_4. It can be seen that not all the voids were detected by microwaves, but these particular voids were also weakly imaged in an X-ray, indicating that they probably contained some kind of material rather than being empty as was intended.

It is interesting to note the partial diffraction pattern produced by the uppermost holes on the left of the scan area. In principle, such a diffraction pattern could provide information about the geometry of the scatterer. The microwave C-scan apparently also shows some inclusions that are not detected in the ultrasonic C-scan.

*Billet No. F307104930.

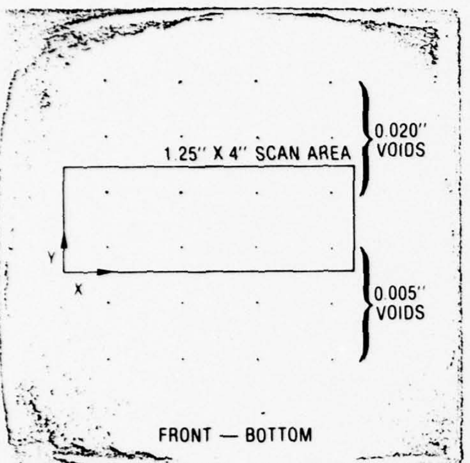

(a) Ultrasonic C-Scan (Focussed 25 MHz) Map Showing Void Locations and Scan Area

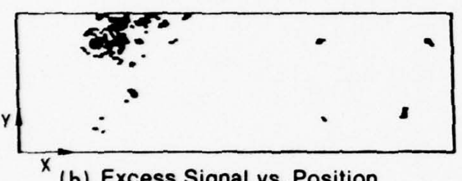

(b) Excess Signal vs. Position

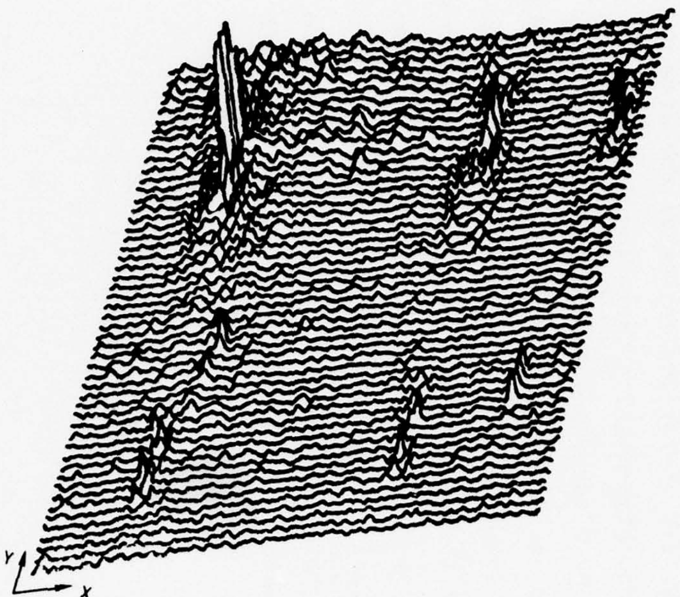

(c) Amplitude vs. Position

L-5594-1

FIGURE 24 MICROWAVE (W-Band) CROSS-POLARIZED-TRANSMISSION C-SCAN SHOWING VOIDS IN HOT-PRESSED Si_3N_4 (frequency = 94 GHz)

Finally, to show the effects of edge scattering, the entire surface of the 4-inch-diameter hot-pressed Si_3N_4 disk (see Figure 5) was scanned with the W-band system. These measurements were made after both surfaces of the disk had been ground smooth. The results are shown in Figure 25. As mentioned in Section IV-B, X-ray inspection of the disk showed the presence of an unintended high-density inclusion. This flaw is clearly detected in the microwave C-scan, and the location of the flaw [see Figure 25(b)] coincides very closely with the location indicated by the X-ray. It can be seen from the figure, however, that the flaw would not have been detectable if it had been near an edge, because the cross-polarized scattering from an edge is quite strong and contributes to the detected signal at a significant distance from the edge. As discussed previously, the region of influence of edge scattering depends on the beamwidth of the antennas, and is minimized when the beamwidth is smallest.

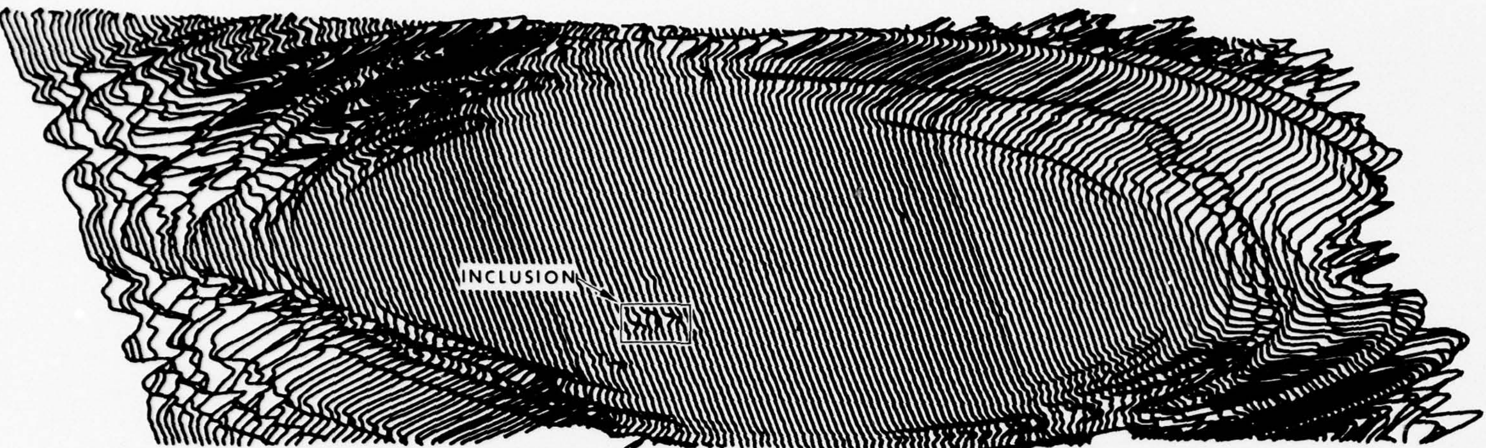

(a) AMPLITUDE vs POSITION

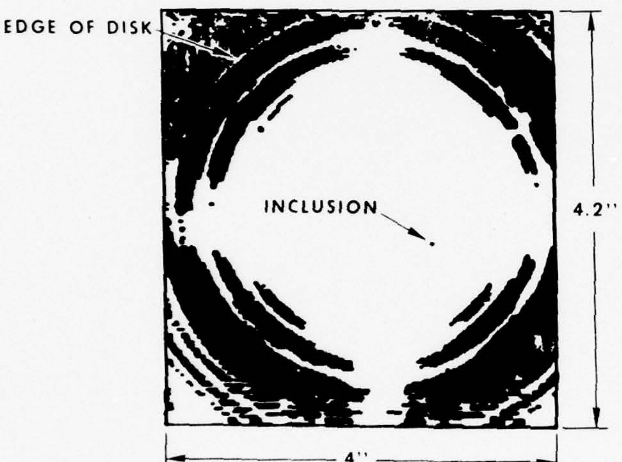

(b) EXCESS SIGNAL vs POSITION

L-5594-2

FIGURE 25 MICROWAVE (W-Band) CROSS-POLARIZED-TRANSMISSION C-SCAN OF 4"-DIAMETER HOT-PRESSED Si_3N_4 DISK (frequency = 94.4 GHz)

V AN OSCILLATOR-PULLING SCHEME FOR DETECTING MICROWAVE BACKSCATTERING FROM A DEFECT

All of the results described in the previous section were obtained from incoherent measurements of the cross-polarized waves scattered forward by a defect in the Si_3N_4. This technique requires the use of two antennas placed directly across from one another on opposite sides of the sample. One difficulty with this arrangement is that the antenna alignment required to maximize the detected signal must be fairly precise. In practice, such alignment will be difficult to achieve because ceramic-turbine parts are not usually in the form of flat plates. The complex geometry of these parts will tend to scatter a transmitted wave into various difficult-to-determine directions. Hence, one would like to use a backscatter detection system where transmitting and receiving antennas are the same physical entity.

Just as in the forward-scatter arrangement, one wishes to separate cross- and co-polarized waves in the backscatter arrangement in order to emphasize defect-related reflections over specular reflections. Two different microwave devices are available for achieving this separation with a single antenna. One device is an isolator that makes use of the principle of Faraday rotation in a ferrite,[16] and the other device is an "orthomode" coupler that separates two orthogonal modes by making use of geometrical differences in their field patterns. The discrimination between orthogonal modes (isolation) is typically 20 dB for an isolator, while an orthomode coupler can achieve an isolation of greater than 30 dB. Thus the latter device should give the best performance, but an isolator was used in the experiments to be described because of its ready availability.

In order to use a typical isolator for separating orthogonally polarized waves, one must remove the rectangular waveguide adapter from the end of the isolator adjacent to the antenna and replace it with a

PRECEDING PAGE NOT FILMED
BLANK

circular waveguide adapter. This permits both orthogonal reflected waves to enter the Faraday-rotation region of the isolator. The cross-polarized wave passes through the isolator, while the co-polarized wave (specular reflection) is absorbed in a resistance card inside the isolator. Of course, the illuminating wave coming from the generator passes through the isolator with very little attenuation.

The backscattered cross-polarized wave separated by the isolator can be detected directly using a directional coupler in the manner shown in Figure 26(a). However, a potentially more sensitive method of detection is to measure the change in generator frequency that is caused by this wave. This scheme is illustrated in Figure 26(b). Although the antenna is schematically depicted as a horn in the figure, the experiments that will be described were actually conducted using the open-ended circular waveguide on the output of the isolator for an antenna.

The amount of oscillator pulling produced by a given amount of reflected wave can be estimated using the theory of Adler.[17] He shows that the fractional change in frequency can be expressed very simply as

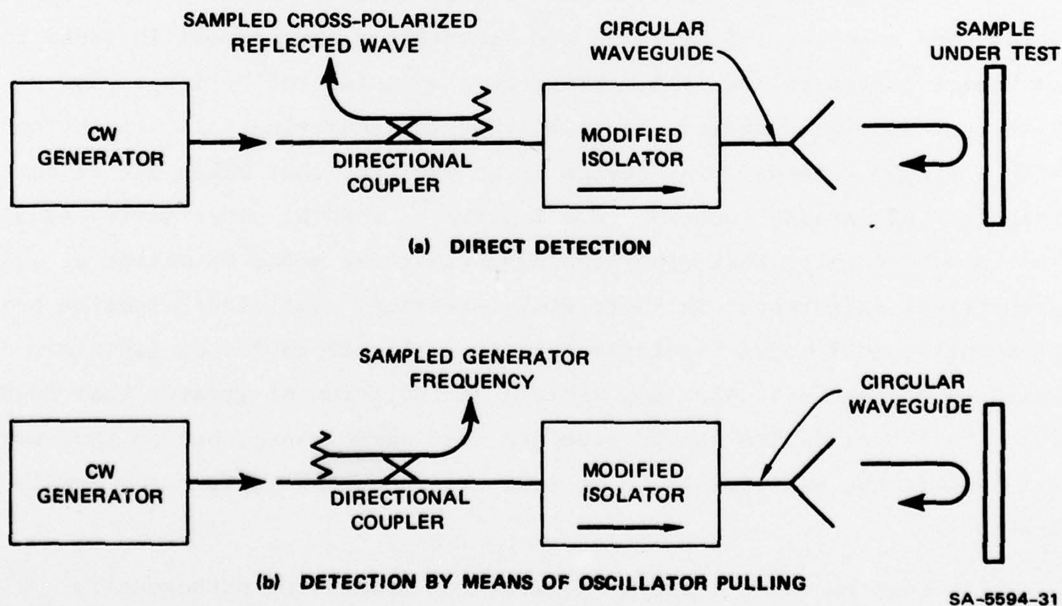

FIGURE 26 TWO MONOSTATIC-BACKSCATTER SCHEMES

$$\Delta f/f_0 = C|\delta| \cos(\alpha + \beta) \quad (7)$$

where

Δf = Frequency shift

f_0 = Unperturbed oscillator frequency

$C\angle\beta$ = Complex coupling constant

$1 + |\delta|\angle\alpha$ = Complex ratio of load impedance to reference impedance.

By definition, the reflection coefficient of the load, Γ, is related to the load impedance by the expression

$$\Gamma = \frac{\delta}{2 + \delta} \quad . \quad (8)$$

If $|\delta| \ll 1$, one finds from Eq. (8) that

$$|\delta| \approx 2|\Gamma| \quad . \quad (9)$$

Now, a typical value for $\Delta f/f_0$ for an IMPATT diode is 0.002 when $|\Gamma|$ = 0.09 (VSWR = 1.2). Assuming this number corresponds to the worst case where $\cos(\alpha + \beta) = 1$, one finds that $C \approx 0.01$. Hence, for this example,

$$(\Delta f/f_0)_{max} \simeq 0.02|\Gamma| \quad . \quad (10)$$

The physical meaning of $|\Gamma|$ in Eq. (8) is that it is the fraction of the incident wave that returns to the generator after it has been back-scattered by a defect. Thus, Eq. (10) can be expressed in terms of the ratio of the reflected power to the incident power, and this relation has been plotted in Figure 27 for f_0 = 100 GHz. It can be seen that a small amount of reflected power at this frequency produces a considerable amount of frequency deviation. Thus the sensitivity of this detection technique appears to be quite good. Moreover, this technique is coherent in that the frequency deviation is dependent on both the amplitude and phase of the reflected wave.

In order to test these ideas, a frequency-pulling arrangement was put together using available equipment. A block diagram of this

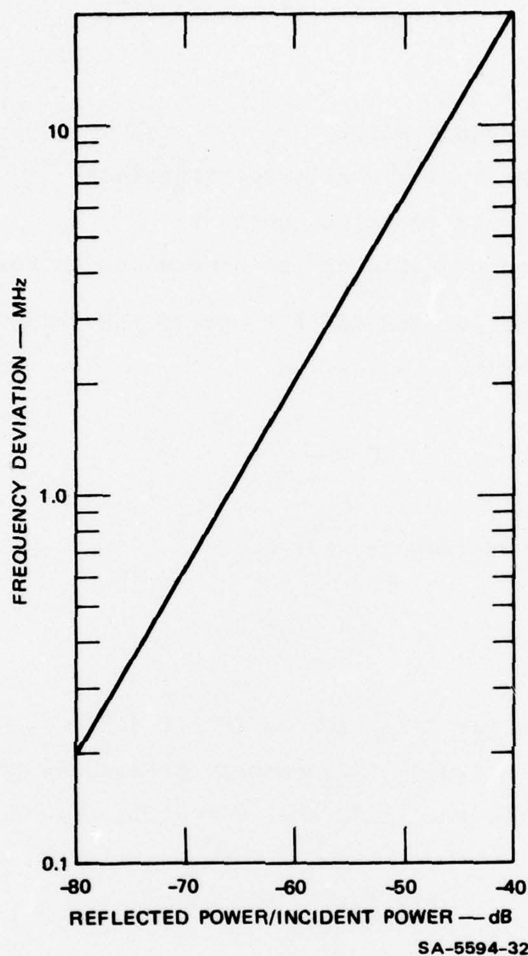

FIGURE 27 FREQUENCY DEVIATION vs RELATIVE REFLECTED POWER FOR f_0 = 100 GHz

experimental arrangement is shown in Figure 28. The fundamental oscillator used in this scheme was a 55-GHz IMPATT source. The system was made sensitive to cross-polarized backscattered waves by using a modified isolator as discussed in connection with Figure 26. Double conversion was used in order to bring the signal down to the UHF band where an available FM receiver could be used. An automatic-frequency-control loop was added when it was found that slow drifts in frequency were a problem.

Rather than using seeded defects in a Si_3N_4 plate, a simple target was devised instead as a preliminary test for the system. This target

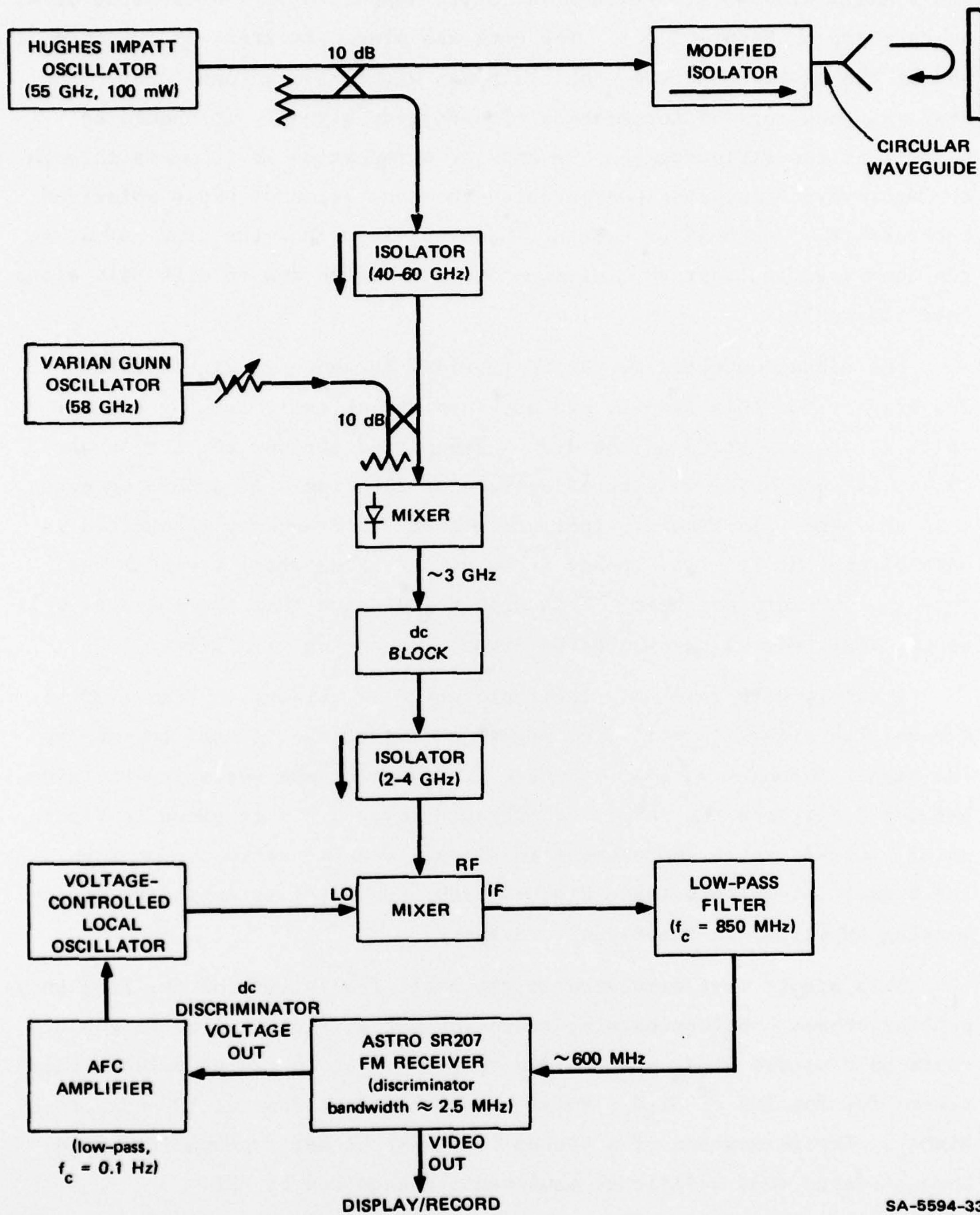

FIGURE 28 EXPERIMENTAL FREQUENCY-PULLING ARRANGEMENT

was a small 0.060-by-1.0-inch metal strip supported on a dielectric disk, as is shown in Figure 29(a). The disk was placed in front of the open end of the isolator so that the strip was within the antenna beam. The disk was then rotated to create a time-varying signal. It should be noted that the strip changes its angular orientation as it moves through the microwave beam, thus guaranteeing the generation of cross-polarized backscatter. One must be careful, however, to orient the disk normal to the beam axis in order to minimize mode conversion due to disk tilt alone (see Figure 1).

The signal detected by the FM receiver is shown in Figure 29(b). The trigger for this display was obtained by optically sensing a small white reflecting strip on the disk. The period for one revolution was 29 ms, corresponding to a rotation rate of 2069 rpm. It should be noted that the signal is bipolar, indicating that the frequency is shifted in both directions from its steady-state value as the metal strip passes through the microwave beam. This result indicates that the phase as well as the amplitude of the scattered signal is varying with time.

A fairly high level of electronic noise is evident in Figure 29(b). Because the signal is periodic, signal averaging can be used to improve the signal-to-noise ratio. A device for sampling and averaging the signal was built, and the result of averaging over 3.7 s is shown in Figure 29(c). Considerable improvement in signal-to-noise ratio can be seen. The signal inversion between Figures 29(b) and 29(c) is caused by an inverting amplifier in the signal averager.

This simple test demonstrates the basic feasibility of the frequency-pulling scheme. Unfortunately, there was not sufficient time to conduct tests on a seeded Si_3N_4 plate. However, in order to truly evaluate this scheme for the NDE of Si_3N_4, these tests should be done at 100 GHz or higher. Implementation of a system for these higher frequencies would have required that additional equipment be acquired by SRI.

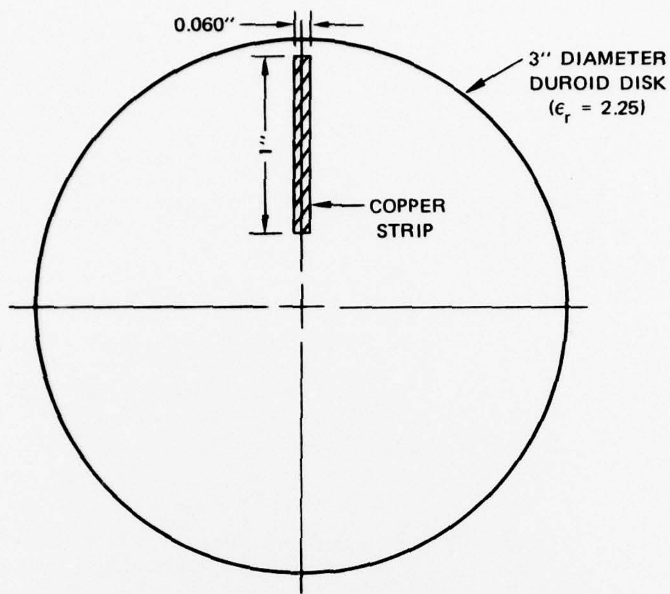

(a) TARGET

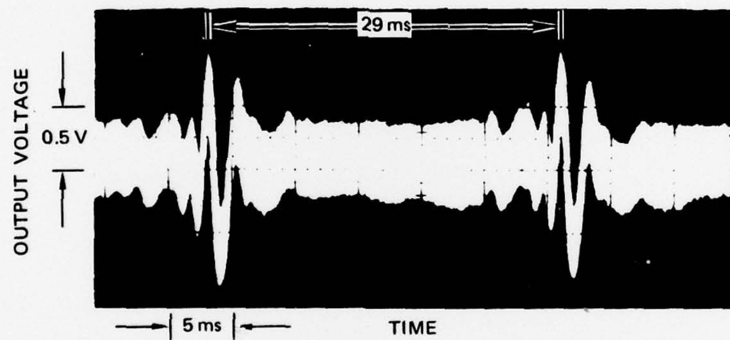

(b) OUTPUT OF FM RECEIVER (no signal averaging)

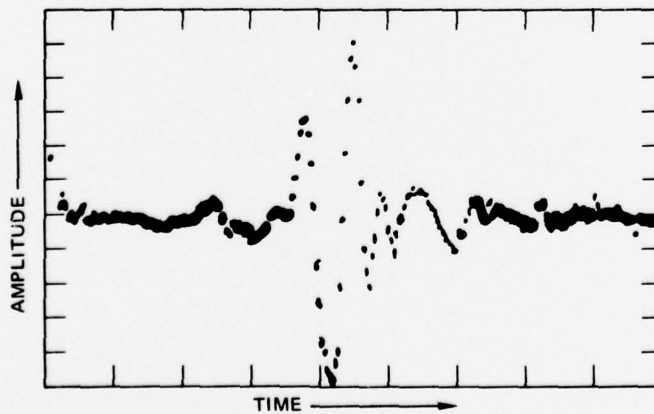

(c) OUTPUT OF FM RECEIVER (averaged over 3.7 s)

SA-5594-34

FIGURE 29 DETECTION OF A METAL STRIP WITH THE FREQUENCY-PULLING SCHEME

VI CONCLUSIONS AND RECOMMENDATIONS

The objective of this study has been to determine the feasibility of using microwave techniques for detecting, locating, and characterizing defects in ceramics, especially hot-pressed Si_3N_4. The work that has been carried out does, in large measure, demonstrate this feasibility. Specific conclusions drawn from this work can be summarized as follows:

- 0.005-inch-diameter defects of various types (including voids) have been successfully detected using frequencies near 100 GHz. Si_3N_4 was found to exhibit very little dissipation loss at these frequencies.
- Microwave scattering appears to be more sensitive to certain types of defects (e.g., unreacted silicon and surface cracks) than are ultrasonic or X-ray techniques. Generally speaking, metallic inclusions were found to produce the largest microwave scattering.
- Using cross-polarized, open-ended waveguides as antennas, local spatial resolutions of a few millimeters were obtained at 100 GHz. Slightly better resolution should be obtainable using lenses.
- A frequency dependence has been observed in the microwave scattering from different types of flaws. This frequency dependence may prove useful for flaw characterization. The need to vary the frequency of the illuminating wave in order to optimize detection and characterization requires that the microwave system be broadband.
- The usable upper frequency of operation for the microwave NDE of ceramics appears to be determined by the background clutter associated with surface roughness and grain boundaries or porosity. This clutter begins to be noticeable at 100 GHz for grit-blasted surfaces and/or reaction-sintered material.
- A limitation of the microwave technique stems from the large amount of scattering that is produced by a sharp geometrical corner. This spurious scattering will mask the weaker scattering produced by any defects in the neighborhood of such a corner.

In general, the most promising microwave technique for the NDE of ceramics appears to be one that makes use of cross-polarized scattering from a defect, either in a forward-scatter or a backscatter mode. Direct

PRECEDING PAGE NOT FILMED
BLANK

incoherent detection of the scattered waves appears feasible. In addition, however, a new detection technique based on oscillator pulling has been demonstrated that appears uniquely suited for NDE, and that may provide greater sensitivity than incoherent detection.

Although the basic feasibility of microwave NDE for ceramics has been demonstrated, further work is required to fully assess the technique. Some of the more important areas worthy of further study are the following:

- Microwave techniques--The work to date has concentrated on forward scattering (transmission) using near-field sensors and incoherent detection (amplitude only). More work is needed to assess the use of backscattering, far-field sensors (using lenses), and phase-sensitive detection.
- Boundary effects--There is a need to study the effect of gently curved surfaces, and the effect of boundaries on the frequency dependence of the scattering.
- Signal interpretation--It is of interest to determine the extent to which one can distinguish between different types of flaws, measure their size and/or shape, and separate adjacent flaws. In general, the limits on location and identification need further quantification.
- Surface cracks--The work so far has concentrated on interior inclusions and voids, but there are indications that microwave techniques may be sensitive to surface defects. The ability of microwave NDE to detect and measure surface cracks (both open and closed) should be evaluated.
- Applications--Some thought should be given to potential application areas for microwave NDE (in the ceramics field). Here, such questions as geometry, material, resolution, cost, reliability, etc., need to be addressed for each specific application.

In summary, the use of microwave techniques for the nondestructive evaluation of Si_3N_4 (and any other ceramic material having similar dielectric properties) appears very promising from a technical standpoint. Of course, acceptance of this technique by the NDE community will depend not only on technical performance, but also on the cost of equipment acquisition. This cost is relatively high at present, but it can be expected to decrease in the future because of the demand that is building in other market areas such as communications, radar, and radiometry.

REFERENCES

1. R. Kossowsky, "Defect Detection in Hot-Pressed Si_3N_4," Ceramics for High-Performance Applications, J. Burke, A. Gorum, and R. Katz, Eds., pp. 665-685 (Brook Hill Publishing Co., Chesnut Hill, Mass., 1974).

2. A. G. Evans, B. R. Tittman, G. S. Kino, and P. T. Khuri-Yakub, "Ultrasonic Flaw Detection in Ceramics," paper presented at the 1976 ARPA/AFML Review of Progress in Quantitative NDE, August 31-September 3, 1976.

3. B. T. Khuri-Yakub and G. S. Kino, "High Frequency Pulse-Echo Measurements of Ceramics and Thin Layers," Proceedings of the 1976 IEEE Ultrasonics Symposium, pp. 564-566 (September 1976).

4. R. Hochschild, "Applications of Microwaves in Nondestructive Testing," Nondestructive Testing, Vol. XXI, pp. 115-120 (March 1963).

5. T. Lavelle, "Microwaves in Nondestructive Testing," Materials Evaluation, Vol. XXV, pp. 254-258 (November 1967).

6. R. J. Botsco, "Nondestructive Testing of Plastics with Microwaves," Materials Evaluation, Vol. XXVII, pp. 25A-32A (June 1969).

7. S. Ramo and J. R. Whinnery, Fields and Waves in Modern Radio, Ch. 7 (John Wiley and Sons, Inc., New York, N.Y., 1953).

8. P. Barber and C. Yeh, "Scattering of Electromagnetic Waves by Arbitrarily Shaped Dielectric Bodies," App. Opt., Vol. 14, pp. 2864-2872 (December 1975).

9. D. E. Barrick, Radar Cross Section Handbook, G. T. Ruck, Ed., Vol. 1, Ch. 3 (Plenum Press, New York, N.Y., 1970).

10. R. J. Hruby and L. Feinstein, "A Novel Nondestructive, Noncontacting Method of Measuring the Depth of Thin Slits and Cracks in Metals," The Review of Scientific Instruments, Vol. 41, pp. 679-683 (May 1970).

11. A. Hussain and E. A. Ash, "Microwave Scanning Microscopy for Non-Destructive Testing," Proceedings of the 5th European Microwave Conference, Hamburg, Germany, pp. 213-217 (September 1975).

12. S. Silver, Ed., "Microwave Antenna Theory and Design," M.I.T. Radiation Lab. Series, Vol. 12, Ch. 11 (McGraw-Hill Book Co., Inc., New York, N.Y., 1948).

13. ibid., Chapt. 10.

14. P. Wong and D. R. Messier, "Dependence of Mechanical and Dielectric Properties of Si_3N_4 on Fabrication Conditions," Am. Ceram. Soc. Bull. (Abstract), Vol. 52, No. 4, p. 427 (1973).

15. W. B. Weir, "Automatic Measurement of Complex Dielectric Constant and Permeability at Microwave Frequencies," Proc. IEEE, Vol. 62, pp. 33-36 (January 1974).

16. R. E. Collin, Foundations of Microwave Engineering, Ch. 6 (McGraw-Hill Book Co., New York, N.Y., 1966).

17. R. Adler, "A Study of Locking Phenomena in Oscillators," Proc. IRE and Waves and Electrons, Vol. 43, pp. 351-357 (June 1946).

DISTRIBUTION LIST

No. of Copies	To
2	Metals and Ceramics Information Center, ATTN: Mr. Harold Mindlin, Director, and Mr. James Lynch, Assistant Director, 505 King Avenue, Columbus, Ohio 43201
12	Commander, Defense Documentation Center, Cameron Station, Alexandria, Virginia 22314
2	Office of the Deputy Chief of Staff for Research, Development and Acquisition, ATTN: DAMA-ARZ-E, DAMA-CSS, Washington, DC 20310
2	Commander, Army Research Office, ATTN: Dr. George Mayer and Mr. J. J. Murray, P. O. Box 12211, Research Triangle Park, North Carolina 27709
6	Commander, U. S. Army Materiel Development and Readiness Command, ATTN: DRCQA-E; DRCQA-P; DRCDE-D; DRCDMD-FT; DRCLDC; DRCMT, DRCMM-M Alexandria, Virginia 22333
8	Commander, U. S. Army Missile Research and Development Command, ATTN: DRDMI-TB, Redstone Scientific Information Center (2 copies); (1 copy) DRDMI-TK, Mr. J. Alley; DRSMI-M; DRDMI-ET, Mr. Robert O. Black; DRDMI-QS, Mr. George L. Stewart, Jr.; DRDMI-EAT, Mr. R. Talley; DRDMI-QP; Redstone Arsenal, Alabama 35809
3	Commander, U. S. Army Troop Support and Aviation Materiel Readiness Command, ATTN: DRSTS-PLE, Mr. J. Corwin (1 copy); (1 copy each) DRSTS-Q and DRSTS-M, 4300 Goodfellow Boulevard, St. Louis, Missouri 63120
9	Commander, U. S. Army Mobility Equipment Research and Development Command, ATTN: DRDME-D; DRDME-E; DRDME-G; DRDME-H; DRDME-M; DRDME-T; DRDME-TQ, DRDME-V; DRDME-ZE; DRDME-N Fort Belvoir, Virginia 22060
2	Commander, U. S. Army Tank-Automotive Materiel Readiness Command, ATTN: DRSTA-Q, Warren, Michigan 48090
12	Commander, U. S. Army Armament Research and Development Command, ATTN: DRDAR-LC, Mr. E. Kelly (1 copy) DRDAR-LCA, Dr. Sharkoff (1 copy) DRDAR-LCE, Dr. Walker (1 copy) DRDAR-QAS, Mr. F. Fitzsimmons (5 copies) DRDAR-SCM, Jr. J. Corrie (1 copy) DRDAR-TSP, Mr. B. Stephans (1 copy) DRDAR-TSS, (STINFO) (2 copies) Dover, New Jersey 07801

No. of Copies	To
1	Commander, Watervliet Arsenal, ATTN: DRDAR-LCB, Mr. T. Moraczewski, Watervliet, New York 12189
4	Commander, U. S. Army Aviation R&D Command, ATTN: DRDAV-EXT; DRDAV-QR; DRDAV-QP; DRDAV-QE; St. Louis, Missouri 63166
4	Commander, U. S. Army Tank-Automotive Research and Development Command, ATTN: DRDTA-RKA, Mr. D. Matichuk (1 copy) DRDTA-RKA, Mr. R. Dunec (1 copy) DRDTA-JA, Mr. C. Kedzior (1 copy) DRDTA-UL (Tech Library) (1 copy) Warren, Michigan 48090
1	Director, U. S. Army Industrial Base Engineering Activity, ATTN: DRXPE-MT, Dr. W. T. Yang, Rock Island, Illinois 61201
1	Commander, Harry Diamond Laboratories, ATTN: DRXDO-EDE, Mr. B. F. Willis, 2800 Powder Mill Road, Adelphia, Maryland 20783
4	Commander, Aberdeen Proving Ground, ATTN: STEAP-MT; STEAP-TL; STEAP-MT-M, Mr. J. A. Feroli; STEAP-MT-G, Mr. R. L. Huddleston; Aberdeen Proving Ground, Maryland 21005
2	Naval Research Laboratory, ATTN: Dr. J. M. Krafft, Code 8430; Library, Code 2620; Washington, DC 20375
3	Director, Air Force Materiel Laboratory, ATTN: AFML-DO, Library; AFML-LTM, Mr. E. Wheeler; AFML-LLP, Mr. R. Rowand; Wright-Patterson AFB, Ohio 45433
20	Director, Army Materials and Mechanics Research Center, ATTN: DRXMR-P (1 copy) DRXMR-PL (2 copies) DRXMR-M (2 copies) DRXMR-MQ (1 copy) DRXMR-MI, Mr. Darcy (1 copy) DRXMR-L, Dr. Chait (1 copy) DRXMR-MI, Mr. Hastings (11 copies) DRXMR-AP (1 copy)
1	R. W. McClung, Metals and Ceramics Division, Oak Ridge National Laboratory, P. O. Box X, Oak Ridge, Tennessee 37803
1	Hughes Aircraft Company, Electron Dynamics Division, ATTN: Dr. Charles A. Escoffery, 3100 West Lomita Boulevard, Torrance, CA 90509
1	Chief, Materials Engineering Department, Dept. 93-03M, AiResearch Manufacturing Company of Arizona, 402 South 36th Street, P. O. Box 5217, Phoenix, AZ 85010

Army Materials and Mechanics Research Center,
Watertown, Massachusetts 02172
MICROWAVE TECHNIQUES FOR
NONDESTRUCTIVE EVALUATION
OF CERAMICS
Alfred J. Bahr
SRI International
Menlo Park, California 94025

Technical Report AMMRC CTR 77-29,
November 1977, 76 pp, Contract DAAG46-
76-C-0048, D/A Project M766350,
AMCMS Code 5397-0M-6350, Final Report,
30 June 1976 to 30 August 1977

AD____________________

UNCLASSIFIED
UNLIMITED DISTRIBUTION

Key Words

Nondestructive evaluation
Microwaves
Silicon nitride
Ceramics

The ability of microwave energy to penetrate some kinds of ceramic materials at frequencies of 100 GHz and above suggests that microwave techniques may be useful for the nondestructive evaluation (NDE) of such materials. The work described in this report demonstrates the basic feasibility of using these techniques to detect and locate various types of inclusions (including voids) in Si_3N_4. Inclusions as small as 0.005 inch in diameter have been detected using frequencies in the range 50 to 100 GHz.

Army Materials and Mechanics Research Center,
Watertown, Massachusetts 02172
MICROWAVE TECHNIQUES FOR
NONDESTRUCTIVE EVALUATION
OF CERAMICS
Alfred J. Bahr
SRI International
Menlo Park, California 94025

Technical Report AMMRC CTR 77-29,
November 1977, 76 pp, Contract DAAG46-
76-C-0048, D/A Project M766350,
AMCMS Code 5397-0M-6350, Final Report,
30 June 1976 to 30 August 1977

AD____________________

UNCLASSIFIED
UNLIMITED DISTRIBUTION

Key Words

Nondestructive evaluation
Microwaves
Silicon nitride
Ceramics

The ability of microwave energy to penetrate some kinds of ceramic materials at frequencies of 100 GHz and above suggests that microwave techniques may be useful for the nondestructive evaluation (NDE) of such materials. The work described in this report demonstrates the basic feasibility of using these techniques to detect and locate various types of inclusions (including voids) in Si_3N_4. inclusions as small as 0.005 inch in diameter have been detected using frequencies in the range 50 to 100 GHz.

Army Materials and Mechanics Research Center,
Watertown, Massachusetts 02172
MICROWAVE TECHNIQUES FOR
NONDESTRUCTIVE EVALUATION
OF CERAMICS
Alfred J. Bahr
SRI International
Menlo Park, California 94025

Technical Report AMMRC CTR 77-29,
November 1977, 76 pp, Contract DAAG46-
76-C-0048, D/A Project M766350,
AMCMS Code 5397-0M-6350, Final Report,
30 June 1976 to 30 August 1977

AD____________________

UNCLASSIFIED
UNLIMITED DISTRIBUTION

Key Words

Nondestructive evaluation
Microwaves
Silicon nitride
Ceramics

The ability of microwave energy to penetrate some kinds of ceramic materials at frequencies of 100 GHz and above suggests that microwave techniques may be useful for the nondestructive evaluation (NDE) of such materials. The work described in this report demonstrates the basic feasibility of using these techniques to detect and locate various types of inclusions (including voids) in Si_3N_4. Inclusions as small as 0.005 inch in diameter have been detected using frequencies in the range 50 to 100 GHz.

Army Materials and Mechanics Research Center,
Watertown, Massachusetts 02172
MICROWAVE TECHNIQUES FOR
NONDESTRUCTIVE EVALUATION
OF CERAMICS
Alfred J. Bahr
SRI International

Technical Report AMMRC CTR 77-29,
November 1977, 76 pp, Contract DAAG46-
76-C-0048, D/A Project M766350,
AMCMS Code 5397-0M-6350, Final Report,
30 June 1976 to 30 August 1977

AD____________________

UNCLASSIFIED
UNLIMITED DISTRIBUTION

Key Words

Nondestructive evaluation
Microwaves
Silicon nitride
Ceramics

The ability of microwave energy to penetrate some kinds of ceramic materials at frequencies of 100 GHz and above suggests that microwave techniques may be useful for the nondestructive evaluation (NDE) of such materials. The work described in this report demonstrates the basic feasibility of using these techniques to detect and locate various types of inclusions (including voids) in Si_3N_4. Inclusions as small as 0.005 inch in diameter have been detected using frequencies in the range 50 to 100 GHz.